ONE-POT SYNTHESIS AND CHARACTERIZATION OF COLLOIDALLY ROBUST RHODIUM(0) NANOPARTICLES CATALYST: EXCEPTIONAL ACTIVITY IN THE DEHYDROGENATION OF AMMONIA BORANE FOR CHEMICAL HYDROGEN STORAGE

A THESIS SUBMITTED TO
THE GRADUATE SCHOOL OF NATURAL AND APPLIED SCIENCES
OF
MIDDLE EAST TECHNICAL UNIVERSITY

BY

TUĞÇE AYVALI

IN PARTIAL FULFILLMENT OF THE REQUIREMENTS
FOR
THE DEGREE OF MASTER OF SCIENCE
IN
CHEMISTRY

JULY 2011

Approval of the thesis:

ONE-POT SYNTHESIS AND CHARACTERIZATION OF COLLOIDALLY ROBUST RHODIUM(0) NANOPARTICLES CATALYST: EXCEPTIONAL ACTIVITY IN THE DEHYDROGENATION OF AMMONIA BORANE FOR CHEMICAL HYDROGEN STORAGE

submitted by **TUĞÇE AYVALI** in partial fulfillment of the requirements for the degree of **Master of Science in Chemistry Department, Middle East Technical University** by,

Prof. Dr. Canan Özgen _____
Dean, Graduate School of **Natural and Applied Sciences**

Prof. Dr. İlker Özkan _____
Head of Department, **Chemistry**

Prof. Dr. Saim Özkar _____
Supervisor, **Chemistry Dept., METU**

Examining Committee Members:

Prof. Dr. Gülsün Gökağaç Arslan _____
Chemistry Dept., METU

Prof. Dr. Saim Özkar _____
Chemistry Dept., METU

Prof. Dr. Deniz Üner _____
Chemical Engineering Dept., METU

Assoc. Prof. Dr. Ayşen Yılmaz _____
Chemistry Dept., METU

Assist. Prof. Dr. Emren Nalbant Esentürk _____
Chemistry Dept., METU

Date: 07.07.2011

I hereby declare that all information in this document has been obtained and presented in accordance with academic rules and ethical conduct. I also declare that, as required by these rules and conduct, I have fully cited and referenced all material and results that are not original to this work.

Name, Last name: Tuğçe AYVALI

Signature:

ABSTRACT

ONE-POT SYNTHESIS AND CHARACTERIZATION OF COLLOIDALLY ROBUST RHODIUM(0) NANOPARTICLES CATALYST: EXCEPTIONAL ACTIVITY IN THE DEHYDROGENATION OF AMMONIA BORANE FOR CHEMICAL HYDROGEN STORAGE

Ayvalı, Tuğçe

M.Sc., Department of Chemistry

Supervisor: Prof. Dr. Saim Özkar

July 2011, 62 pages

The production of transition metal(0) nanoparticles with controllable size and size distribution are of great importance in catalysis since their catalytic activity decreases as nanoparticles aggregate into clumps and ultimately to the bulk metal. Reducing the particle size of heterogeneous catalyst provides a significant rise in its activity as the fraction of surface atoms increases with decreasing particle size. Therefore, transition metal(0) nanoparticles need to be stabilized to certain extend in their catalytic applications by strong stabilizers. In this regard, *tert*-butylammonium octanoate $[(CH_3)_3CNH_3^+][CH_3(CH_2)_6COO^-]$ seems to be an appropriate stabilizer for rhodium(0) nanoparticles since octanoate anion and its associated *tert*-butylammonium cation can provide a sufficient protection for rhodium(0) nanoparticles against aggregation by the combined electrostatic and steric effects.

We report herein the preparation and characterization of rhodium(0) nanoparticles stabilized by *tert*-butylammonium octanoate and their catalytic use in the dehydrogenation of ammonia borane, H_3NBH_3, which appears to be the most promising hydrogen storage material due to its high hydrogen content (19.6 wt %). Rhodium(0) nanoparticles stabilized by *tert*-butylammonium octanoate were reproducibly prepared by the reduction of rhodium(II) octanoate dimer with *tert*-butylamine borane in toluene at room temperature and characterized by EA, XRD,

ICP/OES, TEM, HRTEM, STEM, FTIR, XPS, UV-VIS and NMR spectroscopy. The new rhodium(0) nanoparticles is the first example of well-defined, reproducible, and isolable true heterogeneous catalyst used in the dehydrogenation of ammonia borane. They show record catalytic activity in the dehydrogenation of ammonia borane at room temperature with an *apparent initial* TOF value of 342 h^{-1} and TTO value of 1100.

Keywords: Nanoparticles, Catalyst, Rhodium, Ammonia Borane, Dehydrogenation

ÖZ

HİDROJENİ KİMYASAL OLARAK DEPOLAMAK İÇİN AMONYAK BORANIN DEHİDROJENLENMESİNDE MÜKEMMEL BİR ETKİNLİK SAĞLAYAN KOLLOİDAL SAĞLAMLIKTA RODYUM(0) NANOKÜME KATALİZÖRÜNÜN BİR BASAMAKTA HAZIRLANMASI VE TANIMLANMASI

Ayvalı, Tuğçe

Yüksek Lisans, Kimya Bölümü

Tez Yöneticisi: Prof. Dr. Saim Özkar

Temmuz 2011, 62 sayfa

Geçiş metal(0) nanokümelerinin üretiminin kontrol edilebilir büyüklükte ve büyüklük dağılımında yapılması, katalitik tepkimelerde büyük önem arz etmektedir; çünkü nanokümelerin bir araya gelmesi ve sonunda büyük metal grupları oluşturması katalitik etkinliğin azalmasına neden olmaktadır. Heterojen katalizörlerin parça büyüklüğünü küçültmek, yüzey atom oranını arttıracağından, etkinliğin önemli ölçüde artmasını sağlar. Bu nedenle, geçiş metal(0) nanokümelerinin katalitik uygulamalarda güçlü kararlaştırıcılar ile belli bir ölçüde kararlaştırılması gereklidir. Bu düşünce doğrultusunda, tersiyerbutilamonyum oktanoat ($[(CH_3)_3CNH_3^+][CH_3(CH_2)_6COO^-]$), rodyum(0) nanokümeleri için uygun bir kararlaştırıcı olarak görülebilir; çünkü oktanoat anyonu ve ilgili tersiyerbutilamonyum katyonu, rodyum(0) nanokümelerinin bir araya toplanmasına karşı elektrostatik ve sterik (yapısal) etkilerle yeterli koruma sağlayabilir.

Bu tezde, tersiyerbutilamonyum octanoat ile kararlılaştırılmış rodyum(0) nanokümelerinin hazırlanmasını, tanımlanmasını ve bu nanokümelerin, yüksek hidrojen içeriğinden dolayı (ağırlıkça 19,6%) hidrojen depolamada gelecek vaad eden amonyak boranın dehidrojenlenme tepkimesindeki katalitik etkinliğini sunuyoruz. Tersiyerbutilamonyum ve oktanoat ile kararlaştırılmış rodyum(0) nanokümeleri tecimsel rodyum oktanoat dimerinin, tersiyerbutilamin boranın

dehidrojenasyon tepkimesinde eş zamanlı indirgenmesi yolu ile elde edilmiştir. Hazırlanan rodyum(0) nanokümeleri izole edililerek EA, XRD, ICP/OES, TEM, HRTEM, STEM, FTIR, XPS, UV-görünür elektronik soğurma ve NMR spectroskopik yöntemleri kullanılarak tanımlanmıştır. Bu yeni rodyum(0) nanokümeleri amonyak boranın dehidrojenlenmesinde kullanılan ilk iyi tanımlanmış, tekrarlanabilir ve izole edilebilir gerçek heterojen katalizördür. Bu nanokümeler, oda sıcaklığında amonyak boranın dehidrojenlenmesinde rekor değerlerde başlangıç çevrim frekansı (342 h^{-1}) ve toplam çevirim sayısı (1100) göstermiştir.

Anahtar Kelimeler: Nanokümeler, Katalizör, Rodyum, Amonyak Boran, Dehidrojenlenme

To my family,

ACKNOWLEDGEMENT

I would like to express my sincere gratitude to my supervisor Prof. Dr. Saim Özkar for his priceless support, guidance and encouragement, especially in desperate times, during my graduate studies and in the completion of this dissertation. I am deeply honored to have a chance to work in his laboratory, and to be alumni of his highly respected research group.

I would like to present my special appreciation to Dr. Mehmet Zahmakıran for his guidance, patience, support and motivation throughout my thesis studies and thank to him for his brother-like friendship.

My special thanks to my great friends Melek Dinç, Neval Çelebi, Lütfiye Savcı, Kerem Buran, Svetlana Borukhova and Hatem Efe for their valuable friendship, endless encouragement and motivation in my undergraduate and postgraduate years.

Thanks to my laboratory collaborators Assist. Prof. Önder Metin, Serdar Akbayrak, Huriye Erdoğan, Murat Rakap, Salim Çalışkan, Ebru Ünel, Dr. Mehdi Masjedi, Derya Çelik and Selin Şencanlı for their good friendship and motivation.

Visiting scholars of our research group Feyyaz Durap, Yalçın Tonbul, Senem Karahan, Sibel Duman and Şule Yıldırım are also acknowledged for their support and friendship.

The last but not the least, my special appreciation and great thankfulness are dedicated to my mum İjlal Ayvalı, my dad Ahmet Ayvalı, my sister Ayça Akdeniz and brother-in-law Arda Akdeniz for their love, patience and moral support during the period of my master studies and my nephew Derin Akdeniz for making me happy by his just a little smile. Also thank to my cousin Gökçe Güneş for her moral support and motivation.

TABLE OF CONTENTS

LIST OF FIGURES

FIGURES

LIST OF TABLES

TABLES

LIST OF ABBREVIATIONS

ICP-OES **:** Inductively Coupled Plasma - Optical Emission Spectroscopy

TEM **:** Transmission Electron Microscopy

STEM **:** Scanning Transmission Electron Microscopy

EDX **:** Energy Dispersive X-Ray

XRD **:** X-Ray Diffraction

XPS **:** X-Ray Photoelectron Spectroscopy

FT-IR **:** Fourier Transform Infrared

ATR-IR **:** Attenuated Total Reflectance Infrared

LMCT **:** Ligand to Metal Charge Transfer

F-P **:** Fisher-Porter

Rh(0) NPs **:** *tert*-butylammonium octanoate stabilized rhodium(0) nanoparticles

AB **:** Ammonia borane

TBAB **:** *tert*-butylamine borane

TOF **:** Turnover frequency

TON **:** Turnover number

J **:** Coupling constant

$\mathbf{E_a}$ **:** Activation energy

CHAPTER 1

INTRODUCTION

1.1 The Motivation of This Dissertation

Over the last decade, nano-catalysis has recently attracted intense attention since the nano-sized particles increase the exposed surface area of the active component of the catalyst, thereby enhancing the contact between reactants and catalyst dramatically and mimicking the homogeneous catalysts [1a]. However, their insolubility in reaction solvents makes them easily separable from the reaction mixture like heterogeneous catalysts. Moreover, the activity and selectivity of nano-catalyst can be manipulated by tailoring chemical and physical properties like size, shape, composition and morphology which was previously almost impossible [1a]. In addition to their superior activity and selectivity, nano-catalysts are usually isolable, bottleable and reusable, thus they meet the modern requirements of green catalysis.[2]

Owing to the properties mentioned above, metal nanoparticles have been used in many catalytic reactions such as hydrogenation, dehydrogenation, hydrosilation, McMurry, Suzuki and Heck-Type couplings. Among them, dehydrogenation reactions have aroused interest because hydrogen which is seen as the fuel-of-future is not an energy source but an energy carrier that has to be produced by using energy, starting from hydrogen-rich compounds. [3]

Although, the highest specific energy content possession among all conventional fuels and environmental benignity makes hydrogen as a best candidate for future energy supply, the storage of hydrogen is a challenging issue due to its low

boiling point and low density. One of the promising methods of hydrogen storage is using chemical hydrides. The advantages of storing hydrogen in the form of chemical hydrides include high volume efficiencies, relative ease of recovery, indefinite storage capacities without loss of hydrogen and a high degree of safety. [4]

Particularly, ammonia borane (H_3NBH_3, AB) is a promising solid hydrogen storage material [5] due to its high stoichiometric hydrogen content (19.6 wt %) [6], which is greater than the 2015 target of the U.S Department of Energy (9 wt % hydrogen for a material to be practically applicable), low molecular weight and stability in solid state and in aqueous solution at ambient temperatures.

There have been various reports about AB dehydrogenation in the solid state [7] and in solution [8]. However, thermolysis occurs at temperatures that are too high (around 110, 150 and 1400 ^oC for the first, second and third equivalents of H_2 [9]) and hydrolysis results in toxic metaborate which makes regeneration difficult due to strong B-O bond. Therefore, there is recently much interest in the transition metal catalyzed dehydrogenation of AB due to favorable kinetics and mild reaction conditions. More importantly, recent reports [10] related to the regeneration of dehydrogenation products amplify the importance of the catalytic dehydrogenation of ammonia borane.

Many transition metal catalysts have been tested in the dehydrogenation of AB and as a common feature, all these catalysts, except the unstable $Rh(0)_n$ [11,12] and Pt/Al_2O_3 [13] are homogeneous [14,16-23], **(Table 1)**. Although significant performance in terms of the rate of H_2-release from AB has been achieved by using homogeneous catalysts, such as a pincer-type iridium complex [15,23] and $[Pd(allyl)][BF_4]$ [22], this high activity has a short lifetime. For example, the most recent literature [22] has reported that the high performance, allegedly homogeneous catalyst $[Pd(allyl)][BF_4]$ precipitates out after the first cycle of AB dehydrogenation.

Table 1. Catalyst systems and conditions used in dehydrogenation of ammonia borane.

(Pre)catalyst	Conditions	TOF (h^{-1})	Reference
$[Rh(1,5\text{-}cod)(\mu\text{-}Cl)]_2$	0.4% mol in tetraglyme at 45 ^{0}C	3.3	11
$(POCOP)Ir(H)_2$	0.5% mol in THF at 25 ^{0}C	857	16
$Ni(Ender's\ NHC)_2$	9.1% mol C_6D_6/THF at 60 ^{o}C	10	17
$[(\eta^5\text{-}C_5H_3\text{-}1,3\text{-}(SiMe_3)_2)_2Ti]_2\ (\mu_2\text{-}N_2)$	9.1% mol C_6D_6/THF at 65 ^{o}C	0.23	18
$[Ru(H_2NC_2H_4P^iPr_2)_2Cl_2] + KO^tBu$	0.1% mol in THF at 20 ^{0}C	348	19
$[Ru(H_2NC_2H_4P^tBu_2)_2Cl_2] + KO^tBu$	0.1% mol in THF at 25 ^{0}C	174	19
$[RuH_2(\eta^2\text{-}H_2)_2(PCy_3)_2]$	33% mol in toluene at 25 ^{0}C	-	20
Pt/Al_2O_3	2% mol in diglyme at 70 ^{0}C	250	13
Shvo catalyst	4.8% mol in diglyme/C_6H_6 at 70 ^{0}C	16	21
$[Pd(MeCN)_4]BF_4$	3.0% mol in tetraglyme at 25 ^{0}C	2667	22
$(POCOP)Ir(H)_2$	0.3% mol in THF at 20 ^{0}C	997	23
Rh(0) NPs	1.5% mol in THF at 25 ^{o}C	342	This study

Besides, the synthetic procedures used for the preparation of these homogeneous catalysts are mostly complicated or time-consuming and some problems are involved in product isolation or catalyst recovery due to the homogeneous nature of the catalysis. Because of the advantages of heterogeneous

catalysis [24], current research has been directed toward the development of heterogeneous catalysts possessing high activity.

In the recent studies [25], it has been demonstrated the employment of dimethylammonium hexanoate stabilized rhodium(0) and 3-aminopropyltriethoxysilane stabilized ruthenium(0) nanoparticles as heterogeneous catalysts in the dehydrogenation of dimethylamine borane. They show high activities in the room temperature dehydrogenation of dimethylamine borane, and these results encouraged us to develop transition metal nanoparticles catalyst with high activity and long lifetime in the dehydrogenation of AB using the advantages of semi-heterogeneous catalysis mentioned in Chapter 2. In this regard, rhodium(0) nanoparticles stabilized by *tert*-butylammonium octanoate, hereafter referred to as ***Rh(0) NPs*** were prepared in one-step by the reduction of rhodium(II) octanoate dimer with *tert*-butylamine borane in toluene at room temperature. These Rh(0) NPs were found to be stable enough for being isolated, bottled and reused; in contrast to the dimethylammonium hexanoate stabilized ones [25a].

As summary, in this dissertation, we present our detailed study on the synthesis and characterization of *tert*-butylammonium octanoate stabilized rhodium(0) nanoparticles (Rh(0) NPs) as catalyst for hydrogen generation from the dehydrogenation of AB.

CHAPTER 2

CATALYSIS

2.1 General Aspects of Catalysis

Catalysts have been used by humankind for many years [26]. The first observed uses of catalysts were in making wine, cheese and bread. It was found that it was always necessary to add small amounts of the previous batch to make the current batch [27]. However, the underlying principles of catalysis have not been recognized until 1835. The term *catalysis* was first introduced by the Swedish chemist Jöns Jacob Berzelius in 1835 to tie together the observations of earlier chemists. Berzelius assumed that catalysts possess great power that could affect the course of chemical reactions. [27]

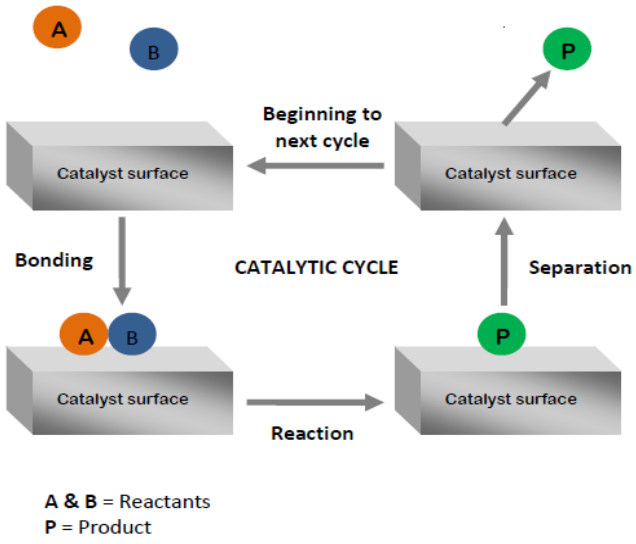

Figure 1. The catalysis cycle and its elementary steps.

In 1894 Oswald restated the explanations of Berzelius and gave a definition to catalyst which is still valid today. A *catalyst* is a substance that speeds up a chemical reaction but emerges from the process as unchanged and *catalysis* is the occurrence, study and use of catalyst and catalytic processes. As the catalyst is not consumed in the catalytic process, each catalyst molecule can take part in many repeated cycles **(Figure 1)**; therefore, using only small amount of catalyst relative to substrate is enough in reactions.

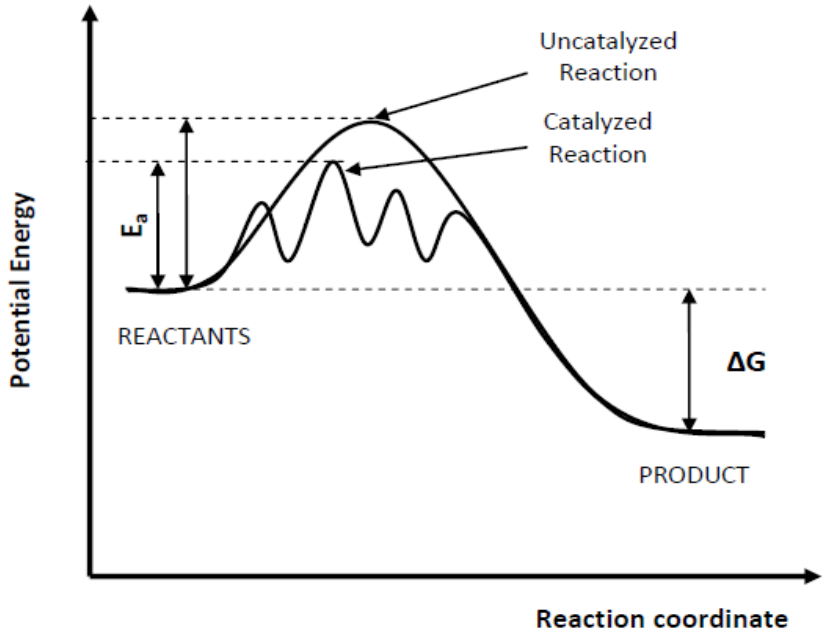

Figure 2. Generic potential energy diagram showing the effect of a catalyst in a hypothetical exothermic chemical reaction.

Catalysts work by providing an alternative molecular path (mechanism) for the reaction involving a different transition state and lower activation energy. Since activation energy is defined as the minimum energy that must be overcome to have a reaction, lowering activation energy barrier leads to more molecular collisions having the energy needed to reach the transition state. Hence, catalysts can enable reactions that would otherwise be blocked or slowed by a kinetic barrier. The catalyst may increase reaction rate or selectivity, or enable the reaction at lower temperatures. This effect can be illustrated with an energy profile diagram shown in **Figure 2**.

In the diagram, the presence of catalyst opens a different reaction pathway with lower activation energy. The final result and overall thermodynamics are the same since the catalysts do not change the extent of a reaction, i.e. they have no effect on the chemical equilibrium because the rate of both forward and reverse reactions are affected.

2.2 Ideal Catalyst for Practical Use

The suitability of a catalyst in order to satisfy industry demands depends mainly on the following three criteria [2,28]:

- Activity
- Selectivity
- Stability

Designing a long-lived, efficient, selective, well-defined, isolable and reusable catalyst is under investigation of various research groups in today's world. In order to achieve such an *ideal* catalyst, all these three criteria have to be satisfied.

2.2.1 Activity

Activity is a measure of how fast one or more reactions proceed in the presence of the catalyst. The catalyst activity can be given by *Turnover Number* (TON) or/and *Turnover Frequency* (TOF) values. TON is defined as total number of moles of product formed per mole of catalyst until deactivation **(Equation 1)**. TOF is the catalytic turnover number per unit time (the number of moles of product per mole of catalyst per unit time) **(Equation 2).**

$$\mathrm{TON} = \frac{\text{mole of product}}{\text{mole of catalyst}} \qquad (1)$$

$$\mathrm{TOF} = \frac{\text{mole of product}}{\text{mole of catalyst } x \text{ time}} \qquad (2)$$

2.2.2 Selectivity

The selectivity of a reaction is the fraction of the starting material that is converted to the desired product. A selective catalyst yields a high proportion of the desired product with minimum amount of the side products. High selectivity plays an important role in industry to reduce waste, the work-up equipment of a plant, and to ensure more effective use of feedstock. [28]

2.2.3 Stability

The chemical, thermal and mechanical stability of a catalyst determine its lifetime in industrial reactors. Catalyst stability is influenced by deactivation of the catalyst caused by aging, poisoning or coking. Catalysts that lose activity during a process can often be regenerated before ultimately being replaced. Today the efficient use of raw materials and energy is the major consideration; therefore, the total catalyst lifetime is of crucial importance for the economics of a process. Sustaining the stability and activity of a catalyst in order to reduce costs are the main two targets of scientists that deal with catalysis nowadays. [27,28]

2.3 The Classification of Catalysts

The classification of catalysts known today can be done according to various criteria like structure, composition, area of application or state of aggregation [28]. The classification of catalysts according to state of aggregation in which they act is given in **Figure 3**.

Among the catalyst systems shown in Figure 3, heterogeneous and homogeneous catalysts are well-known two main types. Catalytic processes that take place in a uniform phase are classified as *homogeneous catalysis.* Homogeneous catalysts are generally well-defined chemical compounds or coordination complexes, which are molecularly dispersed with the reactants in the reaction medium. For instance, the decomposition of hydrogen peroxide in aqueous solution is homogeneously catalyzed by bromide ion or catalase.

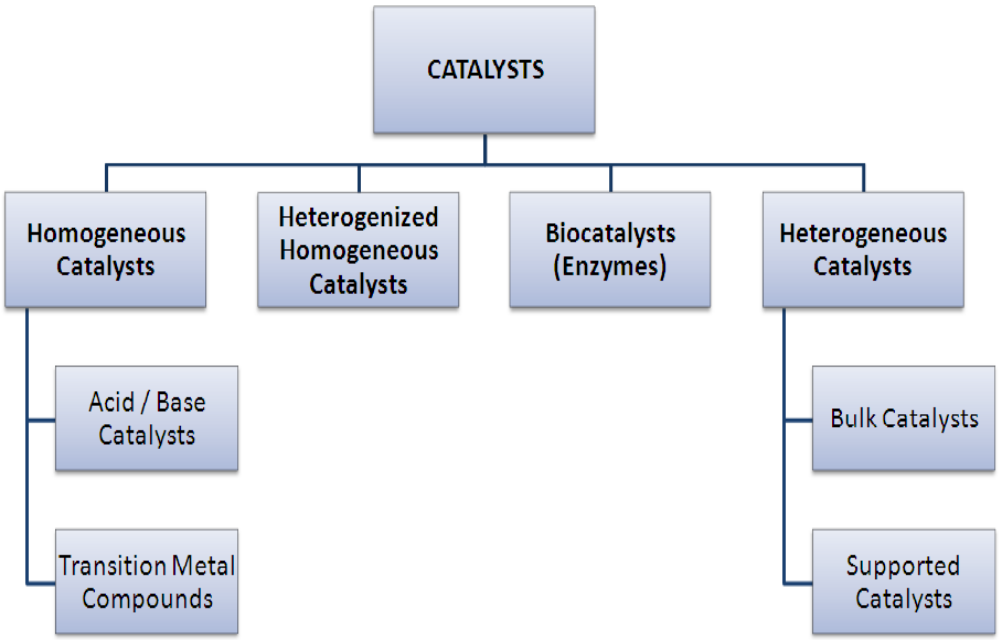

Figure 3. The Classification of Catalysts [28].

In *heterogeneous catalysis*, the catalyst is in a different phase than the reaction mixture. Usually the catalyst is in the solid phase while the reactants are either liquid or gaseous. Although, the separation of the products from the catalyst is relatively easy, the selectivity is less than in homogeneous catalysis. The hydrogenation of ethene to ethane in the presence of platinum, can be given as an example to heterogeneous catalysis.

2.4 Nano-catalysis: A Bridge Between Homogeneous and Heterogeneous Catalysis

The nanoscience has recently come out as a major research route of our modern society resulting from an ongoing effort for miniaturizing the processes that currently use microsystems to the nanoscale. The researchers play their hands in several areas of nanoscience including electronics, biochemical sensors, medicine and catalysis. The latter discipline certainly lies at the hearth of various chemical protocols since a variety of products such as fine chemicals, polymers, fibers, fuels and drugs would not be possible in the absence of catalysts [29].

Heterogeneous catalysis as described in the previous chapter, benefits from easy removal of catalyst materials and possible use of high temperatures; on the other hand, it suffers from reduced contact between catalyst and substrate, lack of selectivity and understanding of the mechanistic aspects of the reactions [1,2]. Homogeneous catalysis has advantages that all catalytic sites are accessible as the catalyst is in the same phase with the reactants. They are usually well-defined, thus by implementing a structure-reactivity relationship, rational development of more efficient catalyst systems can be achieved for a given reaction [2]. Moreover, homogeneous catalysts benefits from high selectivity, better yield and mild operation conditions. However, the difficulty of removal of the catalyst from the reaction media, which is essential in pharmaceutical industry, and their limited thermal stability emerge as two drawbacks of homogeneous catalysis.

2.4.1 Why nano-catalysis is needed?

Green catalysis aspects now desire that environmentally friendly catalysts that allow rapid and selective chemical transformations coupled with easy catalyst removal from the reaction media and recycling many times with very high efficiency be designed [30]. These challenging conditions bring a new research movement for catalyst development at the frontier between homogeneous and heterogeneous catalysis known as *nano-catalysis* (**Figure 4**). The field of nano-catalysis involves both the homogeneous and heterogeneous catalysis communities and therefore, nanocatalysts are sometimes called as *semi-heterogeneous* or *quasi-homogeneous* catalysts [2,31].

The term “nano-catalysis” may be misunderstood by the readers since one may argue that catalysis already occurs on the active sites of atoms in a basic structural unit of materials. However, nano-catalysis is used frequently in the literature [1,2,47] to describe the catalytic processes performing with nano-sized structures ranging from 1-100 nm. Similarly, in this dissertation we use “nano-catalysis” to express catalytic reactions performed by materials (generally metals) in nanoscale regime, somewhere between the bulk solid and molecular state.

The nano-sized particles increase the exposed surface area of the active component of the catalyst, thereby enhancing the contact between reactants and catalyst dramatically and mimicking the homogeneous catalysts. However, their insolubility in reaction solvents makes them easily separable from the reaction mixture like heterogeneous catalysts, which in turn makes the product isolation stage effortless. Furthermore, the activity and selectivity of nanocatalyst can be managed by altering chemical and physical properties like size, shape, composition and morphology. [1a]

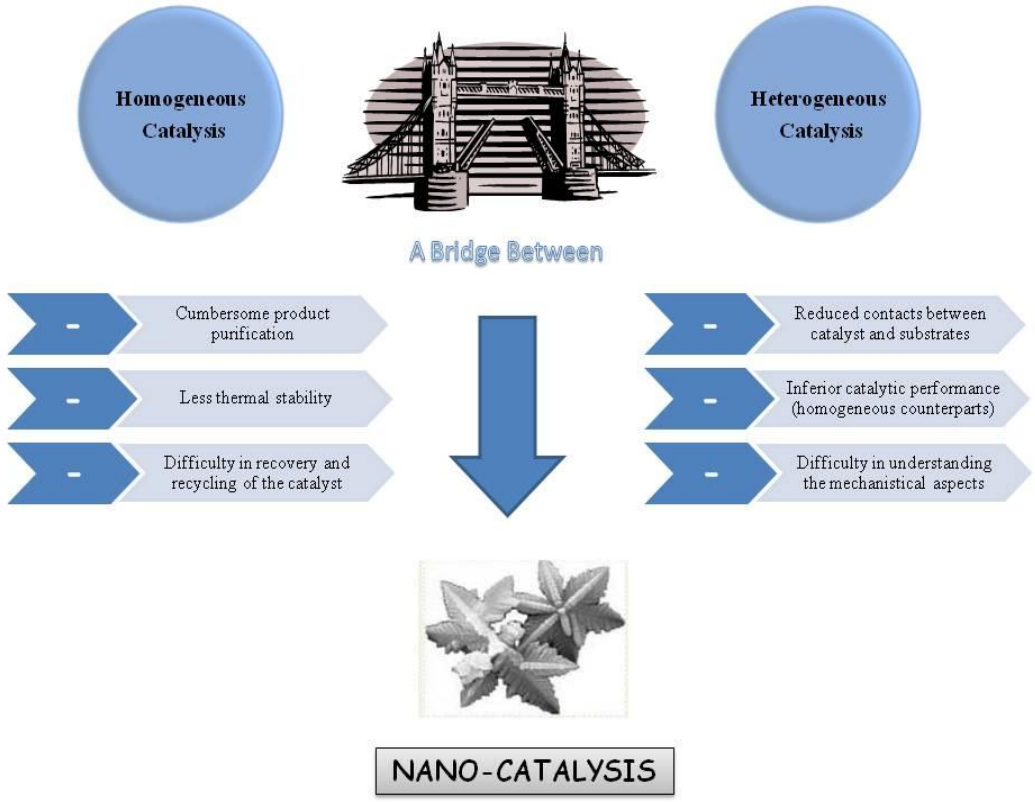

Figure 4. Nanocatalysis: A bridge between homogeneous and heterogeneous catalysis. [1a]

CHAPTER 3

TRANSITION METAL NANOPARTICLES IN CATALYSIS

3.1 Basic Definitions

It should be noted that in the literature nanomaterials are named in different forms such as nanocrystals, nanoparticles, nanoclusters and nanocolloids. In this chapter a short set of definitions will be stated for clarity before starting to explain metal nanoparticles.

Nanocrystals are defined as single crystals with sizes from a few nm up to about 100 nm [32]. Nanocrystals can have relaxed or contracted lattices, and unusual reactivity relative to their larger counterparts.

Nanoparticles are units of minerals, mineraloids or solids smaller in size than 100 nm, and composed of nanocrystals, nanoclusters or other molecular units, and combinations of these. [33]

Nanoclusters are individual molecular units that have well-defined structure, but too small to be true crystals. They have a near-monodispersed size distribution (≤15%), in the range of 1-10 nm. [34]

Nanoporous materials are substances with pores or voids having nanoscale dimensions. These materials can be single crystals, such as zeolites or molecular sieves with cage-like nanopores. Nanoporous solids have unique abilities to encapsulate, bind and react with other nanoparticles and nanoclusters, as well as molecules. [33]

Colloidal particles can have dimensions from small clusters of atoms up to about 10 μm in diameter. They are classically defined as any suspended fine particles in a solvent. Hence smaller colloidal particles are the same as nanoparticles and they are also called as *nanocolloids*.

Although different sources refer to different nanomaterial names; in order to avoid semantic problems, the term 'nanoparticles' will be used throughout this dissertation to denote any type of metallic species with a size between 1 and 50 nm.

3.2 Introduction to Transition Metal Nanoparticles

In the nanoscale regime, somewhere between the bulk solid and molecular state, metal nanoparticles show unique properties with their size ranging from 1 to 50 nm. The unique material properties in this size range come from several sources [35]:

i. *quantum size effect*, where the confinement of charge carriers in a small space leads to discrete energy levels
ii. *classical charging effects*, originating from the discrete nature of the electrical charge
iii. *surface/interface effect*, where the properties of surface or interface atoms become much more significant, as the surface to volume ratio increases with decreasing of particle size.

Metal nanoparticles do not follow classical physical laws as all bulk materials do. They exhibit so-called ''nano-effects'' when reaching a critical size. For instance, the melting point of a solid element or a chemical compound in a classical sense is a constant under distinct conditions whereas this is not the case in nanoparticles. The melting point of bulk gold is known to be 1064 ^{0}C. However, gold nanoparticles below ca. 20 nm in diameter begin slowly to melt at lower temperatures and the melting point then dramatically falls down at a size of 3–4 nm [35,36] as seen in **Figure 5**. The reason for this phenomenon can simply be explained as while the particles are getting smaller, the percentage of surface atoms becomes larger. Since these surface atoms are less nicely coordinated than inner

atoms, they are easily mobilized with increasing temperatures which results in lower melting point.

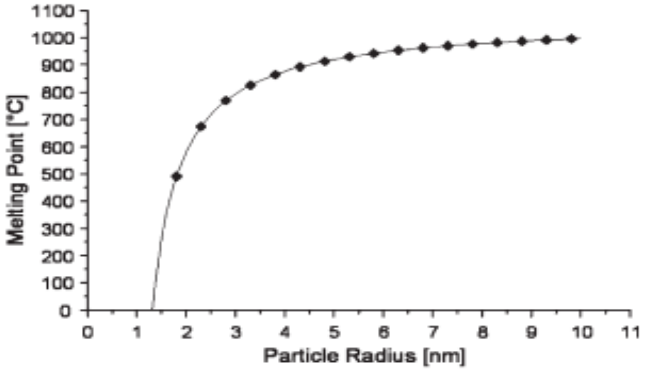

Figure 5. Melting point behaviour of gold nanoparticles [35].

Reducing the size of a metal also affects the color of metal drastically. For example, the color of bulk gold is yellow; on the other hand, if bulk gold is downsized to ca. 50 nm, the yellow color spontaneously disappears and turns to blue, further reduction results in purple and finally bright red colors. This dramatic color change is a consequence of the appearance of plasmon resonances **(Figure 6)**. Plasmon resonances, quantitatively described by the Mie theory [35,37], are caused by the interaction of light with the confined electron gas in such small particles, resulting in a collective electron oscillation. The frequency of this oscillation depends on the kind of metal, the size of the corresponding particles, their shape and the surrounding medium.

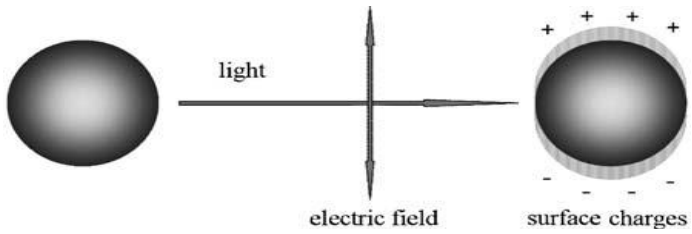

Figure 6. Illustration of the interaction of visible light and the confined electron gas of a metal nanoparticle, resulting in a plasmon resonance [35].

Due to their unique properties mentioned above, the metal nanoparticles have many potential uses such as quantum dots [38], quantum computers [39], chemical

sensors [40], light emitting diodes [41] and industrial lithography [42]. Nanoparticles also have been used in catalysis for over 50 years as they mimic metal surface activation and catalysis at the nanoscale and thereby bring selectivity and efficiency to heterogeneous catalysis. Compared to their bulk counterparts, metal nanoparticles have much higher surface-to-volume ratio, thus, larger fraction of catalytically active atoms on the surface. More importantly, metal nanoparticles provide the possibility of controlling both the particle size and surface composition/modification in quantitative way. In addition to their superior activity and selectivity, metal nanoparticles are usually isolable, redispersible and reusable catalysts. Some examples of catalytic reactions that nanoparticles have been tested and found to be active include hydrogenations [43], dehydrogenations [25], hydrosilyations [44], McMurry [45], Suzuki [46] and Heck-Type [46] couplings.

3.3 Stabilization of Metal Nanoparticles

Although metal nanoparticles are very active in catalysis, they are only kinetically stable. At short interparticle distances, two particles would be attracted to each other by van der Waals forces and, in the absence of any repulsive forces to counteract this attraction, an unprotected sol would coagulate. Therefore, they have to be stabilized in a certain extent against aggregation into larger particles and eventually to bulk metal. There have been many articles about the mode of stabilization of nanoparticles reported in the literature. [47,48] The stabilization of metal nanoparticles is generally divided into five categories namely; electrostatic, steric, electrosteric, ligand stabilization and stabilization on supported materials.

3.3.1 Electrostatic Stabilization

Electrostatic stabilization results from the electrical double layer formed by the anions and cations interacting with the metallic particle surface. This results in columbic repulsion between individual particles that prevents agglomeration. Ionic compounds such as halides [47c,49] or carboxylates [25a,50] could be used to

achieve electrostatic stabilization. **Figure 7** represents a schematic illustration of electrostatic stabilization of metal nanoparticles.

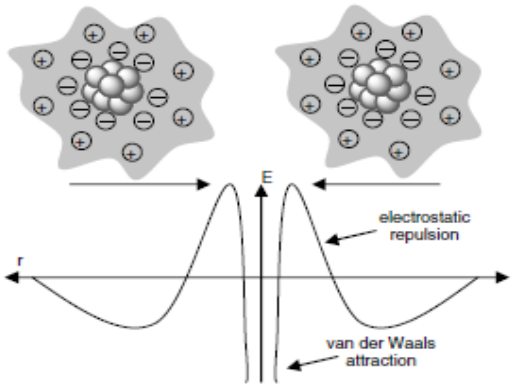

Figure 7. Illustration of electrostatic stabilization of metal nanoparticles [47a].

A dispersion of metal clusters that are only stabilized electrostatically can, however, coagulate easily if the ionic strength of the dispersing medium is increased sufficiently for the double layer to become compressed. The level of stabilization can be influenced by altering the total charge on the metal cluster surface or the polarity of the solvent. [35]

3.3.2 Steric Stabilization

Steric stabilization is achieved by surrounding the metal center by layers of material that are sterically bulky such as polymers [51], surfactants [52] or dendrimers [53], **(Figure 8)**. These large adsorbates provide a steric barrier between metal nanoparticles, thus prevent agglomeration.

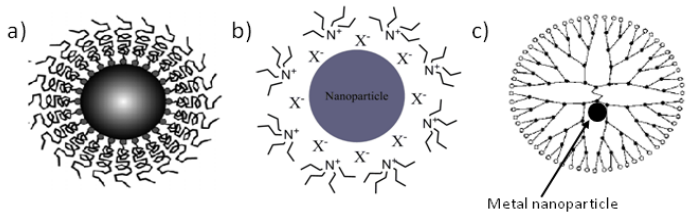

Figure 8. Representations of a) polymer b) surfactant and c) dendrimer stabilized metal nanoparticles

3.3.3 Electrosteric Stabilization

In this kind of stabilization, the combination of both electrostatic and steric effects provides stabilization around metal nanoparticles like in the case of polyoxoanion-stabilized nanoclusters [25a,54]. **(Figure 9)**

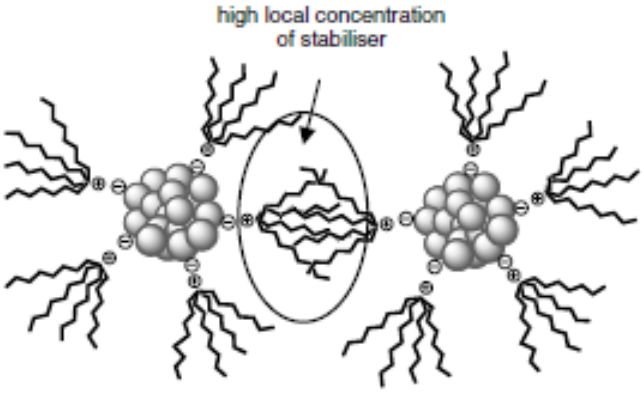

Figure 9. Electrosteric stabilization of metal nanoparticles [47a].

3.3.4 Ligand Stabilization

The predominantly covalent interactions between the ligand molecule and the nanoparticle usually stabilize the particles to such an extent that they may be isolated in solid state, without aggregation. S, P, N, donors of thiols, phosphines and amines respectively can be used as ligands while stabilizing the metal nanoparticles.

3.3.5 Stabilization on Solid Supports

Immobilizing the nanoparticles with confined void spaces of the solid supports such as metal oxides [55], zeolites [56] or metal organic frameworks [57] also represents a promising way to prevent aggregation. Such solid supports are under investigation of many research groups in the world nowadays.

3.4 Synthesis of Metal Nanoparticles

Nanostructured metal colloids are obtained on the basis of two approaches: top-down and bottom-up methods. The top-down method involves the mechanical grinding of bulk metals and subsequent stabilization of the resulting nano-sized metal particles by adding protecting agents [35]. Metal vapor technique for the production of metal nanoparticles is one of the methods used frequently in top-down approach. However, top-down approach suffers from broad particle size distribution (typically larger than 10 nm) and irreproducibility. The more common and practical bottom-up approach involves first the generation of metal atoms and then the nucleation and growth of them to a certain size. The detailed explanations of some common nanoparticle preparation methods by using bottom-up approach are given below.

3.4.1 Reduction of Metal Salts

In this approach **(Equation 3)**, the metal salt precursor is mixed with a reducing agent such as hydrogen, alcohol, hydrazine or borohydride in the presence of stabilizing agents like ligands, polymers or surfactants.

$$x\mathrm{M}^{n+} + nx\mathrm{e}^{-} + \text{stabilizer} \longrightarrow \mathrm{M_n}^{0}{}_{(\text{cluster})} \qquad (3)$$

The reducing agents generate zerovalent metal colloids while the stabilizing agents are preventing the undesired agglomeration and formation of metal powders, **(Figure 10)**. The actual size of the nanoparticles depends on many factors including the type of reducing agent, metal precursor, solvent, concentration, temperature and reaction time.

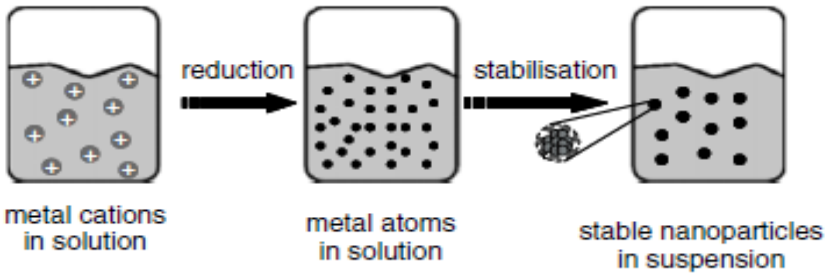

Figure 10. Formation of nanoparticles via metal salt reduction. [47a]

3.4.2 Electrochemical Synthesis

Obtaining stable metal nanoparticles by electrochemistry was developed by Manfred Reetz in 1990s. The overall process includes five steps **(Figure 11)** [47a]:

1. Oxidative dissolution of the sacrificial metal bulk anode
2. Migration of metal ions to the cathode
3. Reductive formation of zerovalent metal atoms at the cathode
4. Nucleation and growth of metal particles
5. Arresting the growth process and stabilizing the nanoparticles with protecting agents.

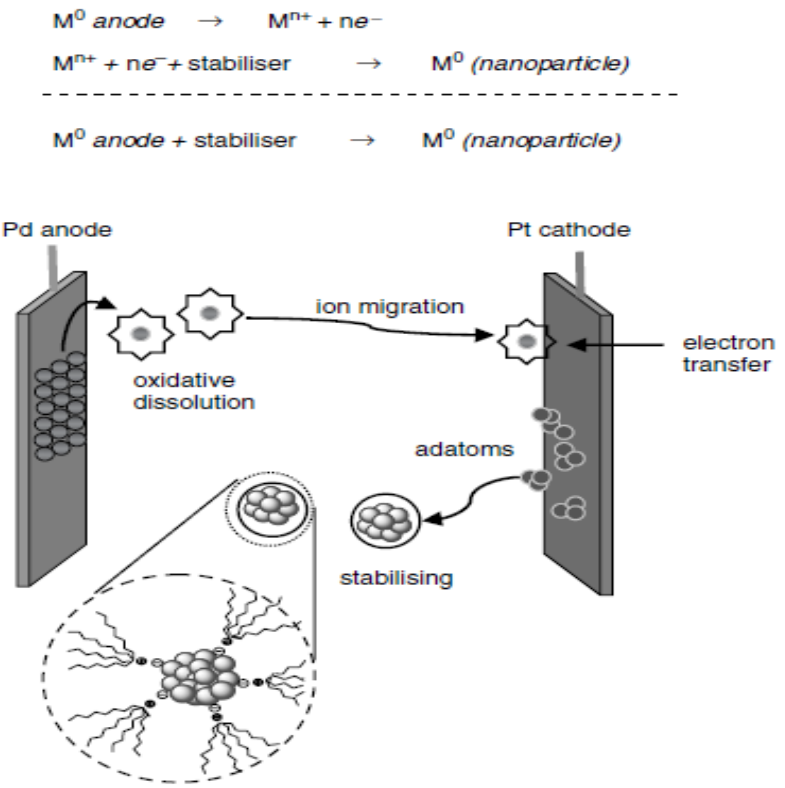

Figure 11. Electrochemical synthesis of $NR_4^+Cl^-$ stabilized Pd nanoparticles [47a,58].

The electrochemical synthesis method has advantage over chemical reduction methods by avoiding the contamination of nanoparticles with by-products. Moreover, it allows size-selective particle formation by tuning the current density or adjusting the distance between the electrodes.

3.4.3 Ligand Reduction from Organometallics

In this method, the ligands are reduced with H_2 or CO starting from low-valent metal complexes. The reduced ligands leave the zerovalent metal center and allow the clustering of metal atoms. **(Equation 4)**

$$n\mathrm{M(L)}_x + x\mathrm{H}_2 + \text{stabilizer} \longrightarrow \mathrm{M}_n{}^0{}_{(\text{cluster})} + x\mathrm{LH}_2 \qquad (4)$$

Some nontraditional methods like microemulsion, laser ablation and gamma radiation used for preparing metal(0) nanoparticles can also be found in the literature.

3.5 Mechanism of Nanoparticle Formation

In the previous chapter, the stabilization and synthesis methods of metal nanoparticles were mentioned. However, one can wonder the mechanistic steps of nanoparticle formation; therefore in this chapter, a brief, general information about the formation mechanism of nanoparticles will be discussed.

Starting with Turkevich [59] who established the first reproducible standard procedure for the preparation of metal colloids, many valuable scientists [15] proposed a mechanism for the stepwise formation of nanoclusters. However, the first well-defined and detailed mechanistic study about the formation of metal nanoclusters was done by Finke et al. [15] during 1990s. Generally the mechanistic formation of metal nanoparticles is based on three steps namely, nucleation, growth, and agglomeration. **(Figure 12)**

The metal salt is first reduced to give zerovalent metal atoms. These atoms collide in solution with further metal(0) atoms or with sub-clusters that have already been formed to give a stable ‘seed’ nucleus of 13 metal atoms [60]. This is the first member of the so-called full-shell cluster family [47b] and its formation is irreversible. To initiate nucleation, the concentration of metal atoms in solution must be high enough to reach supersaturation. After nucleation, the autocatalytic surface growth starts to occur. If the growth period is almost the same for all the particles, a monodisperse sample will be obtained. However, if nucleation and growth do

overlap, then the duration of the growth period will differ between nucleation sites, resulting in an unwanted broad particle size distribution. The growth period has to be stopped by a factor since some time later, the nanoparticles start to coagulate and eventually form aggregated bulk metal. Therefore, in order to gain high-quality nanoparticles, the passivation of the metallic surface by adding stabilizers, as mentioned in Chapter 3.3, is essential. Surface passivation helps to achieve size selectivity by preventing agglomeration and fusing of particles.

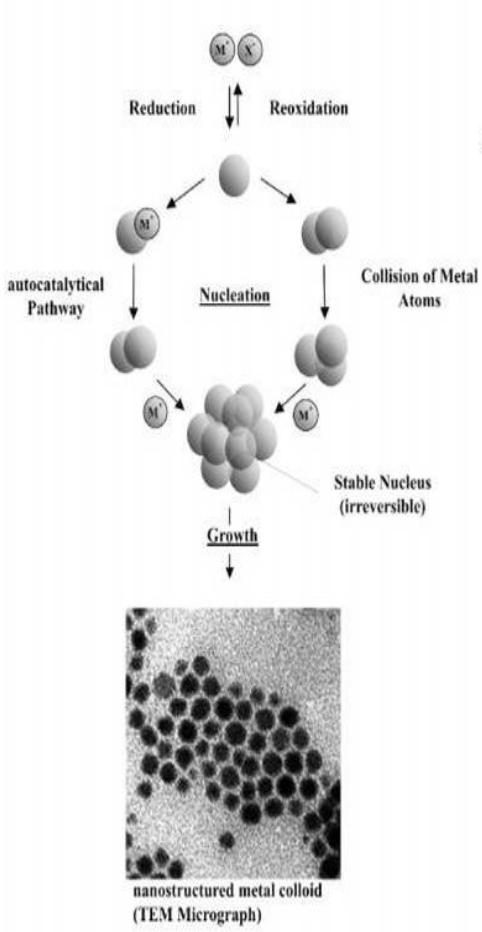

$nM^+ \rightarrow M^0_n$ (reduction of metal salt and formation of nucleus)

$M^0_n + M^+ \rightarrow M^0_{n+1}$ (autocatalytic surface growth)

$M^0_n + M^0_m \rightarrow M^0_{n+m}$ (agglomeration)

Figure 12. Formation of nanostructured metal colloids by the ‘‘salt reduction” method [60].

3.6 Characterization of Transition Metal Nanoparticles

Understanding the physico-chemical behavior of metal nanoparticles and their properties entirely can only be achieved by identifying the size, structure and composition of nanoparticles. All these properties of nanoparticles cannot be measured with a single method; on the contrary, many complementary characterization techniques have to be applied. **Figure 13** represents a scheme which provides a good overall picture of the techniques used to characterize metal nanoparticles.

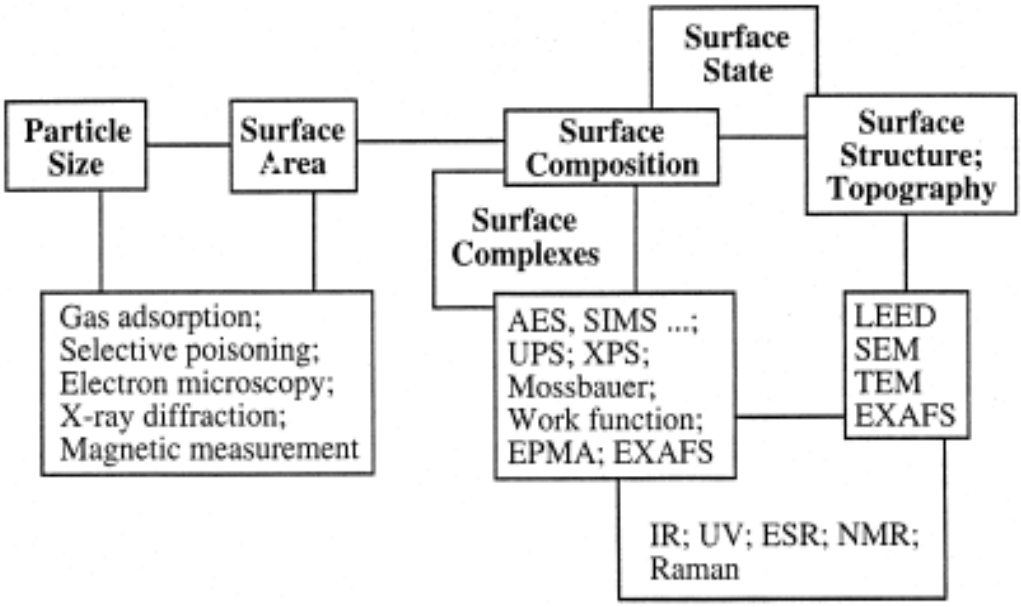

Figure 13. Common methods used to characterize metal nanoparticles. [47b]

Among these techniques showed by Figure 12, the most frequently used methods are transmission electron microscopy (TEM), scanning electron microscopy (SEM), X-ray diffraction (XRD), X-ray photoelectron spectroscopy (XPS), UV-Visible spectroscopy (UV-VIS), nuclear magnetic resonance (NMR) and infrared spectroscopy (IR).

CHAPTER 4

HYDROGEN: AN ENERGY CARRIER

4.1 World Energy Problem

Current energy consumption of world is based on combustion of carbon-based fuels; however, it is known that oil, natural gas and carbon will not last forever [3]. Indeed, the world is faced with the depletion of fossil fuels within coming years since the resources of petroleum and natural gas that take tens of millions of years to form and accumulate have been consumed so rapidly. More importantly, the harsh usage of carbon-based fuels leads to detrimental environmental effects due to the emission of harmful carbon, sulfur and nitrogen oxides which are blamed for global warming and climate change. Therefore, presenting alternative energy sources is essential. An alternative fuel must be technically feasible, economically competitive, environmentally acceptable and readily available [4]. In this manner, among the proposed alternative energies such as biodiesel, electricity, solar fuels, methanol, ethanol etc., hydrogen is the most promising fuel because of having the highest specific energy content of all conventional fuels and being environmentally benign since its combustion produce only water.

Hydrogen is the most abundant element in the universe and exists as invisible, nontoxic diatomic molecule gas. Owing to its high reactivity, hydrogen in nature is nearly always combined with other elements; that is, it is not a primary energy existing freely in the nature. Hydrogen is not an energy source but an energy carrier that has to be produced by using energy, starting from hydrogen-rich compounds [3].

Although hydrogen seems to be the solution of world energy problem, there are still some concerns about hydrogen storage, transportation and distribution.

4.2 Storage of Hydrogen

Hydrogen storage is still a challenging issue that has to be solved as it affects the future hydrogen economy. However, storing hydrogen for both stationary and mobile applications is complicated because of very low boiling point (20.3 K) and low density (0.08 kg/m^3 in gas phase and 71 kg/m^3 in liquid phase) of hydrogen [9]. Compared to hydrocarbons, hydrogen gas has a good energy density by weight (33.3 Wh/kg) but a poor energy density by volume (2.5 Wh/L) [3,61]. As a result of this, hydrogen needs about 3000 times larger space than gasoline having energy density of 8.7 kWh/L [3] for an equivalent amount of energy, under normal conditions. In stationary applications, including industrial and domestic uses, hydrogen storage systems can occupy a relatively large space and their weight is not a major factor. However, hydrogen storage in transportation is limited by volume and weight. To decrease the space needed to store required amount of hydrogen some modifications have to be applied.

At present, hydrogen can be stored physically by changing its state conditions such as temperature, pressure and phase, and chemically in various solid and liquid compounds. In addition, it can also be stored by physisortion on porous organic solids.

4.2.1 Hydrogen Storage by Physical Methods

There are mainly two physical options for storage of hydrogen namely liquid hydrogen storage and compressed hydrogen storage.

i. Liquid Hydrogen Storage

Hydrogen which is one of the most difficult gases to liquefy requires a complex and expensive multistage cooling procedure. About 30-40% of the energy

content of the hydrogen is needed in order to liquefy it at -253 ^{o}C (20 K). Moreover, insulation the liquid hydrogen in tanks is usually very expensive and delicate [3,61]. Any hydrogen leaking from the tank may cause major safety hazards since hydrogen is highly flammable and explosive gas.

ii. Compressed Hydrogen Storage

Although, the storage of hydrogen by compressing is more relevant way of storing it as liquid, it is still far from being satisfactory. Hydrogen can now be held under 35.5 MPa or 71 MPa in tanks made up of new composite light materials such as carbon fiber with metal or polymer liners [62]. However, even at 71 MPa, hydrogen has 4.6 times lower per-volume energy content than gasoline has which means that the hydrogen tank must be much larger.

4.2.2 Hydrogen Storage by Physisorption

Physisorption takes place on most porous organic solids such as carbon nanotubes, activated carbon, metal organic frameworks or zeolites. Physisorption of hydrogen on surfaces is governed by van der Waals interactions between hydrogen molecule and surface of the adsorbent; however, since the van der Waals forces are rather weak, no significant amount of hydrogen can be stored at ambient temperature and pressure [62]. Hydrogen can be adsorbed only as a monolayer at a temperature equal or higher than the boiling point of hydrogen (20.3 K), hence a multi-layer coverage at room temperature (298 K) cannot be expected because the storage temperatures are far above the boiling point of liquid hydrogen.

Recent studies [63] show that materials with very high pore volumes do not necessarily adsorb much hydrogen, whereas hydrogen storage is dominated by small pores with narrow size distribution since hydrogen has lower interaction energy with the wide pores compared with smaller micropores. Therefore materials having high surface areas and large micropore volumes contribute much in storing hydrogen. For instance MOF-177 [64] has an estimated Langmuir surface area of 4500 m^2/g and storage capacity of 7,5 wt% at 7 MPa and 77 K.

4.2.3 Hydrogen Storage by Chemical Methods

An optimum hydrogen storage material must have the following criteria [4]:

1. High volumetric/gravimetric hydrogen storage capacity
2. Fast absorption kinetics
3. Near room temperature and ambient pressure operation
4. Light weight materials
5. Low cost materials

Luckily, some chemical hydrides satisfy most of these criteria. They have an advantage of being compact, requiring less space than compressed hydrogen, working at moderate temperature and pressure, having low molecular weight and high hydrogen content. Moreover, most of chemical hydrides can easily be recovered again since they can be reformed from their products.

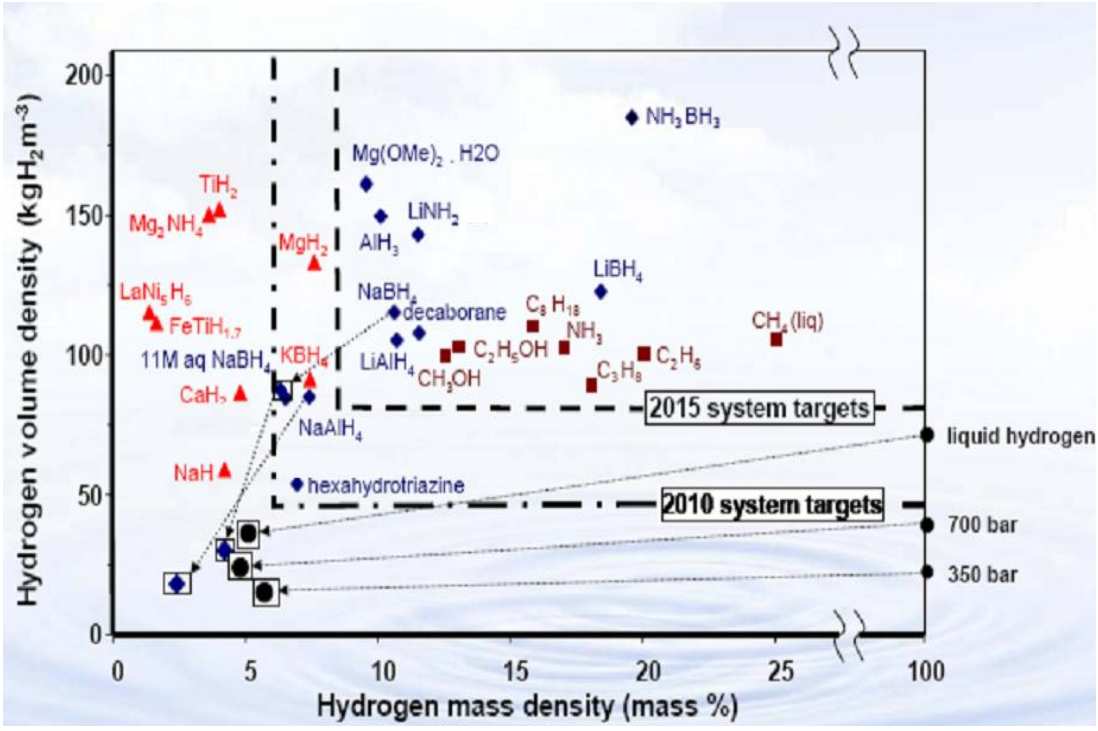

Figure 14. The graph of hydrogen mass density versus hydrogen volume density of some chemical hydrogen storage materials. [46b]

Among the hydrogen containing compounds given in **Figure 14**, ammonia borane seems (AB, NH_3BH_3) to be the most prominent hydrogen storage material due to its high volumetric and gravimetric hydrogen contents (152 g_{H2}/L, 19.6 wt % respectively). AB is stable in solid state and in aqueous solution at ambient temperatures. Having an impressive gravimetric hydrogen capacity, it is potentially capable of meeting U.S. Department of Energy (DOE) targets. (The 2015 target of U.S. DOE includes gravimetric capacity of 9 wt% hydrogen for a material to be practically applicable [6].)

CHAPTER 5

EXPERIMENTAL

5.1 Materials

All commercially obtained compounds were used as received unless indicated otherwise: rhodium(II) octanoate dimer, *tert*-butylamine borane, ammonia borane, tetrahydrofuran, toluene, hexane, methanol, toluene-d_8, quartz NMR sample tubes (Norell S-500-QTZ) were purchased from Sigma–Aldrich. Mercury (99.9%) was purchased from Atalar Chem. Ind. Toluene, THF and methanol were distilled over Na, Na/benzophenone and Mg, respectively, and stored in a nitrogen atmosphere drybox. Deuterated NMR solvent toluene-d_8 was transferred into the drybox for NMR sample preparations therein. All reactions and manipulations were performed under an atmosphere of dry nitrogen using standard Schlenk techniques or in a Labsconco glovebox (<1 ppm O_2) filled with dry nitrogen unless otherwise specified.

5.2 Preparation and Characterization of *tert*-butylammonium octanoate Stabilized Rhodium(0) Nanoparticles (Rh(0) NPs)

5.2.1 Synthesis of Rh(0) NPs

A solution of rhodium(II) octanoate was prepared by dissolving 7.5 μmol of $[Rh(O_2CC_7H_{15})_2]_2$ (5.84 mg, 15 μmol Rh) in 4 mL of toluene in a Schlenk tube by gentle warming. In another Schlenk tube 150 μmol *tert*-butylamine borane (13.4 mg $(CH_3)_3CNH_2BH_3$) was weighed and dissolved in 1 mL toluene. This solution was then transferred by a cannula into a jacketed Schlenk tube which had been evacuated

for at least 30 min to remove any trace of oxygen and water present and brought to constant temperature by a circulating water bath thermostated at 25 ± 0.1 ^{o}C. Then the solution of rhodium(II) octanoate was added to the jacketed Schlenk tube rapidly *via* a cannula. The reaction was started by stirring the mixture at 750 rpm and continued for 2 h **(Figure 15)**. The solution changed its color from green to dark brown. The solution was then concentrated by solvent evaporation before cold hexane addition to favor the colloid precipitation, and the supernatant solution was removed by filtration. The solid was further washed with hexane (3x20 mL) and dried under vacuum, yielding the colloid as a dark brown powder.

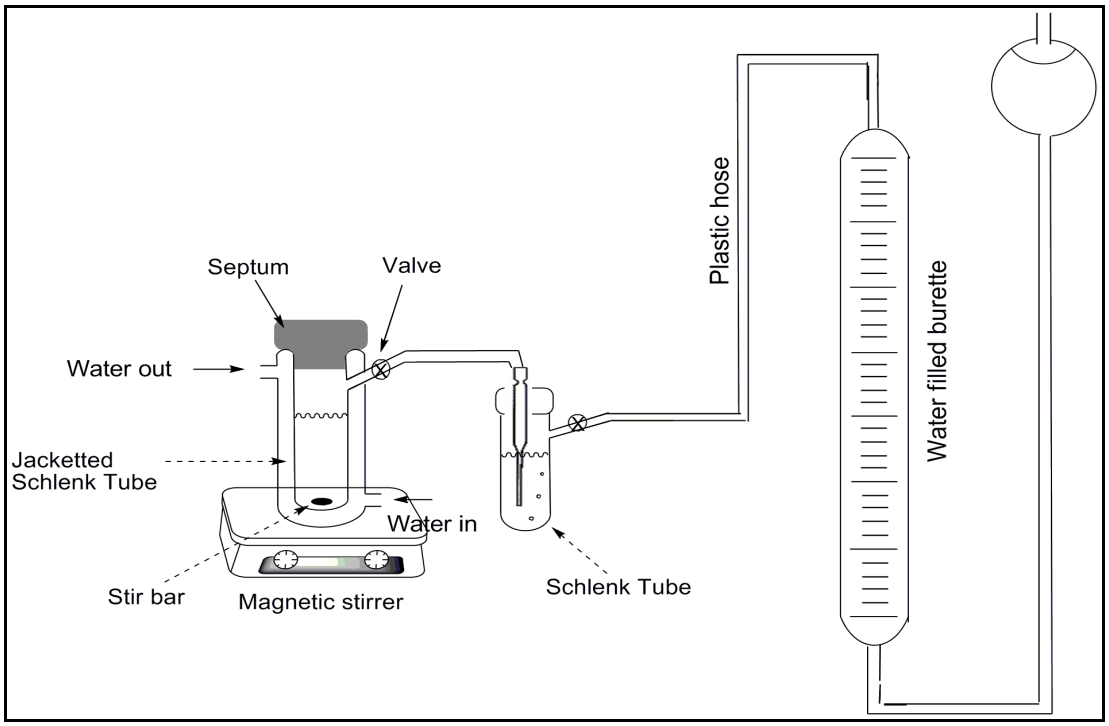

Figure 15. Experimental set-up for the preparation of Rhodium(0) Nanoparticles.

5.2.2 Characterization of Rh(0) NPs and *tert*-butylamine borane Dehydrogenation Products

^{11}B NMR Spectroscopy: The synthesis of rhodium(0) nanoparticles was performed under the same conditions given in the previous section and the gaseous outlet of the reaction solution in the Schlenk tube was bubbled through 10 mL dry methanol in another Schlenk tube, whose outlet was also connected to a graduated

glass burette filled with water to measure the volume of the hydrogen gas to be evolved from the reaction **(Figure 15).**

At the end of the reaction, ^{11}B NMR spectra of the reaction solution and methanol trap were monitored with a Bruker Avance DPX 400 spectrometer with an operating frequency of 128.2 MHz. $BF_3{\cdot}(C_2H_5)_2O$ was used as an external reference for ^{11}B NMR chemical shifts.

^{13}C NMR Spectroscopy: The reaction solution was prepared as described above in toluene-d_8 and ^{13}C NMR spectra were recorded on a Bruker Avance DPX 400 spectrometer with an operating frequency of 100.6 MHz. TMS was used as an internal reference for ^{13}C NMR chemical shifts.

UV-VIS Spectroscopy: UV-VIS electronic absorption spectra were recorded on a Varian Cary 5000 UV-Vis-NIR spectrophotometer.

ICP-OES Analysis: The rhodium content of Rh(0) NPs sample was determined by ICP-OES analysis (Leeman-Direct Reading Echelle) after the sample was dissolved completely in the mixture of HNO_3/HCl having 1 to 3 ratio.

Elemental Analysis: The elemental analysis of Rh(0) NPs sample was done on LECO, CHNS-932.

FT-IR Spectroscopy: The isolated sample of rhodium(0) nanoparticle powders was diluted with KBr (1/10) and pressed into a wafer of 15 mm diameter by using an applied pressure of 6–8 tons per square inch for less than 60 s. Then the FTIR spectrum of rhodium(0) nanoparticles sample spectra were taken from a KBr pellet on a Nicolet Magna-IR 750 spectrometer using Omnic software.

XRD Analysis: The powder XRD pattern was recorded on a MAC Science MXP 3TZ diffractometer using Cu Kα radiation (wavelength 1.5406 Å, 40 kV, 55 mA).

XPS analysis: XPS analysis was performed for the isolated samples of rhodium(0) nanoparticles on a Physical Electronics 5800 spectrometer equipped with a hemispherical analyzer and using monochromatic Al Kα radiation (1486.6 eV, the X-ray tube working at 15 kV, 350 W and pass energy of 23.5 keV).

TEM, STEM and EDX analysis: Rhodium(0) nanoparticles samples were harvested from the reaction solution on a chloroform cleaned carbon coated copper grid by dipping it into solution for 5 s and evaporating the volatiles under N_2 flow. Then the morphology of nanoparticles was monitored on a FEI Tecnai G^2 (X-Twin) microscope with an accelerating voltage of 100 kV (2Å resolution). Particle size analysis was performed using the public domain NIH Image J 1.62 program developed at the U.S. National Institutes of Health and available at http://rsb.info.nih.gov/nih-image/. For each particle, the diameter was calculated from the area by assuming that nanoclusters are spherical. Size distributions are quoted as the mean diameter ± the standard deviation.

5.3 Rh(0) NPs Catalyzed Dehydrogenation of Ammonia Borane

5.3.1 Method of Data Handling

Ammonia borane dehydrogenation catalyzed by Rh(0) NPs was performed in a Fischer–Porter (F–P) pressure bottle connected to a line through Swagelock TFE-sealed quick connects and to an Omega PX-302 pressure transducer interfaced through an Omega D1131 digital transmitter to a computer using the RS- 232 module **(Figure 16).** The progress of an individual dehydrogenation reaction was followed by monitoring the increase in the pressure of H_2 gas on LabVIEW 8.0 program. The catalytic activity of Rh(0) NPs was determined by measuring the rate of hydrogen generation.

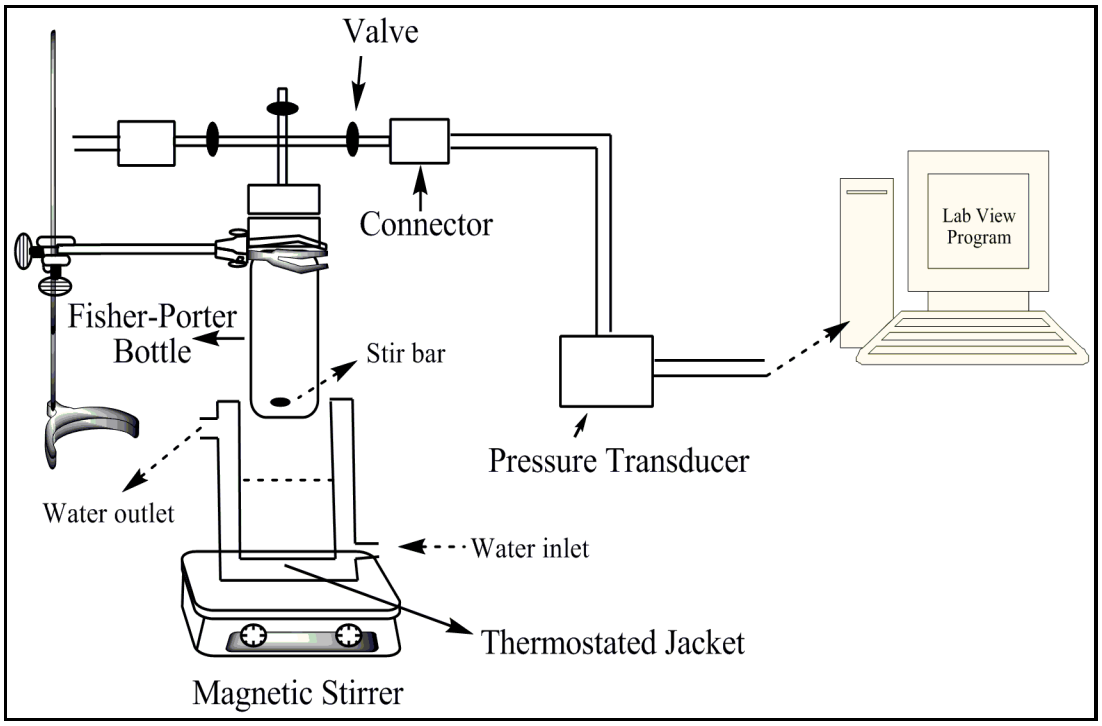

Figure 16. Experimental set-up for dehydrogenation of ammonia borane.

In a typical reaction 1 mmol AB (32 mg H_3NBH_3) was weighed and added into a new 22 x 175 mm pyrex culture tube containing a new 5/16 in. x 5/8 in. teflon coated magnetic stir. The culture tube was then sealed inside the F–P pressure bottle and brought outside the drybox and placed inside a constant temperature circulating water bath thermostated at 25 ± 0.1 ^{o}C unless otherwise specified. Next, the F–P bottle was attached to the line, which had already been evacuated for at least 30 min to remove any trace of oxygen and water present, *via* its TFE-sealed Swagelock Quick-Connects. Under nitrogen purging (14 mL dry N_2 / s) Rh(0) NPs solution in THF (thermostated at 25 ± 0.1 ^{o}C) was added into a F–P pressure bottle rapidly *via* the tap of the bottle by using a 10 mL pyrex volumetric pipette (nitrogen flushed). The pressure inside the F–P bottle was monitored on a PC using LabVIEW 8.0 program. When the pressure inside the F–P bottle established the constant value the reaction was started (t = 0 min.) by stirring the mixture at 500 rpm. When no more hydrogen generation was observed, the experiment was stopped and the F–P bottle was sealed, disconnected from the line and H_2 pressure was released. Then F–P bottle was transferred back into the drybox, a 9 in. glass Pasteur pipette was used to

withdraw a *ca.* 0.5 mL aliquot from the culture tube. This reaction solution aliquot was then transferred into a NMR sample tube which was subsequently sealed and then brought out of the drybox for the ^{11}B NMR analysis. The raw pressure *vs.* time data collected with the computer interfaced transducer were exported from LabVIEW 8.0 and imported into OriginPro 8. Before any fitting was done, the raw data from experiments carried out in THF were corrected for the build up of pressure in the F–P bottle due to the solvent vapor pressure and initial N_2 pressure then converted into the values in proper unit, volume of hydrogen (mL).

5.3.2 Reusability of Rh(0) NPs

At the end of the dehydrogenation of 150 μmol ammonia borane (4.8 mg H_3NBH_3) catalyzed by 30μmol Rh(0) NPs at 25 ± 0.1 ^oC, the F–P bottle was sealed, disconnected from the line and H_2 pressure was released and transferred into the drybox then dispersed on a chloroform cleaned carbon coated copper grid for TEM analysis by dipping it into solution for 5 s and evaporating the volatiles under N_2 flow. Next, the reaction solution was transferred into a new Schlenk tube which was subsequently sealed and brought out of the drybox. The solution was precipitated with cold hexane (10 mL), which was added into this solution under N_2 atmosphere, and the supernatant solution was removed by filtration. The solid was further washed with hexane (3 x 20 mL) and dried under vacuum, giving then rise to the colloid as a dark brown powder (^{11}B NMR analysis of its dispersion in THF shows that the surface of rhodium(0) nanoparticles are free from polymeric $(BNH)_x$ dehydrocoupling products) which was then redispersed in THF and used again in the dehydrogenation of 150 μmol AB under the same conditions as in the first run.

5.3.3 Catalytic Lifetime Experiment

The catalytic lifetime experiment was started with 5 μmol Rh(0) NPs and 10 mmol ammonia borane (320 mg H_3NBH_3) in THF at 25 ± 0.1 ^oC. When no more hydrogen generation was observed, a new batch of AB was added into the F–P bottle

under N_2 purging and the experiment was continued until no hydrogen evolution was observed.

5.3.4 Hg(0) Poisoning Experiments

Two sets of experiments were performed; in the first set elemental Hg (0.3 g, 1.5 mmol, *ca.* 200 equiv) was added into 7.5 μmol Rh(0) NPs solution in the nitrogen filled dry-box and the mixture stirred for 4 h. Then, this solution was used in the dehydrogenation of 1.0 mmol AB (32 mg, H_3NBH_3) at 25 ± 0.1 °C. In the second set, when ~45% of conversion in AB dehydrogenation, started with 7.5 μmol Rh(0) NPs + 1.0 mmol AB, was reached, elemental Hg (0.3 g, 1.5 mmol, *ca.* 200 equiv) was added into the reaction solution under N_2 purging.

5.4 Catalytic Activity of Rhodium(II) Octanoate Precatalyst and Insoluble bulk Rhodium(0) in the Dehydrogenation of Ammonia Borane

5.4.1 Catalytic Dehydrogenation of Ammonia Borane Starting with Rhodium(II) Octanoate Precatalyst

The catalytic dehydrogenation of 1.0 mmol AB (32 mg H_3NBH_3) was performed by using 7.5 μmol $[(CH_3(CH_2)_6CO_2)_2Rh]_2$ in THF at 25 ± 0.1 °C in the same way as described in the section of 5.3.1 "Method of Data Handling". After the release of 0.6 equivalent of H_2 within 1 h, insoluble agglomerates were formed and precipitated out from the solution.

5.4.2 Testing the Activity of Insoluble bulk Rhodium(0) Formed from the Ammonia Borane Reduction of Rhodium(II) Octanoate Dimer

At the end of reduction of 7.5 μmol $[(CH_3(CH_2)_6CO_2)_2Rh]_2$ with 1.0 mmol AB (32 mg H_3NBH_3) at 25 ± 0.1 °C, the F–P bottle was sealed, disconnected from the line and H_2 pressure was released and transferred into the drybox, the reaction solution containing precipitates was filtered and precipitates were transferred into a new Schlenk tube (5 mL) which was subsequently sealed and brought out of the

drybox. Then, insoluble Rh(0) was dried under vacuum (10^{-3} Torr) for 3 h at room temperature. The activity of insoluble Rh(0) was tested in the dehydrogenation of 0.1 mmol AB (3.2 mg H_3NBH_3) in THF at 25 ± 0.1 ^oC in the same way as described in previous sections. The insoluble bulk Rh(0) found to be catalytically inactive for the dehydrogenation of ammonia borane; no detectable hydrogen generation was observed over 10 h.

CHAPTER 6

RESULTS AND DISCUSSION

6.1 Synthesis and Characterization of *tert*-butylammonium octanoate Stabilized Rhodium(0) Nanoparticles

Rh(0) NPs were prepared in a schlenk tube by the reduction of rhodium(II) octanoate dimer ($[Rh(O_2CC_7H_{15})_2]_2$) with *tert*-butylamine borane (TBAB, $(CH_3)_3CNH_2BH_3$), whereby a molar ratio of [TBAB]/[Rh] = 10 was used to ensure the complete reduction of rhodium(II) to its zerovalent state. The gaseous outlet of the reaction solution in Schlenk tube was bubbled through 10 mL dry methanol in another Schlenk tube, whose outlet was also connected after a check valve to the a graduated glass filled with water to measure the volume of the hydrogen gas to be evolved from the reaction. So that, the progress of rhodium(0) nanoparticle formation and concomitant dehydrogenation of *tert*-butylamine borane was followed by monitoring the changes in hydrogen pressure.

Figure 17 shows conversion *versus* time plot for the dehydrogenation of TBAB starting with $[Rh(O_2CC_7H_{15})_2]_2$ precatalyst in toluene at $25 \pm 0.1\ ^0C$. The sigmoidal kinetic curve has been shown to be characteristic for nanoparticle formation reactions [25b,15]:

$$nRh(II) \rightarrow Rh_n(0) \text{ (nucleation)}$$

$$Rh(II) + Rh_n(0) \rightarrow Rh_{n+1}(0) \text{ (autocatalytic surface growth)}$$

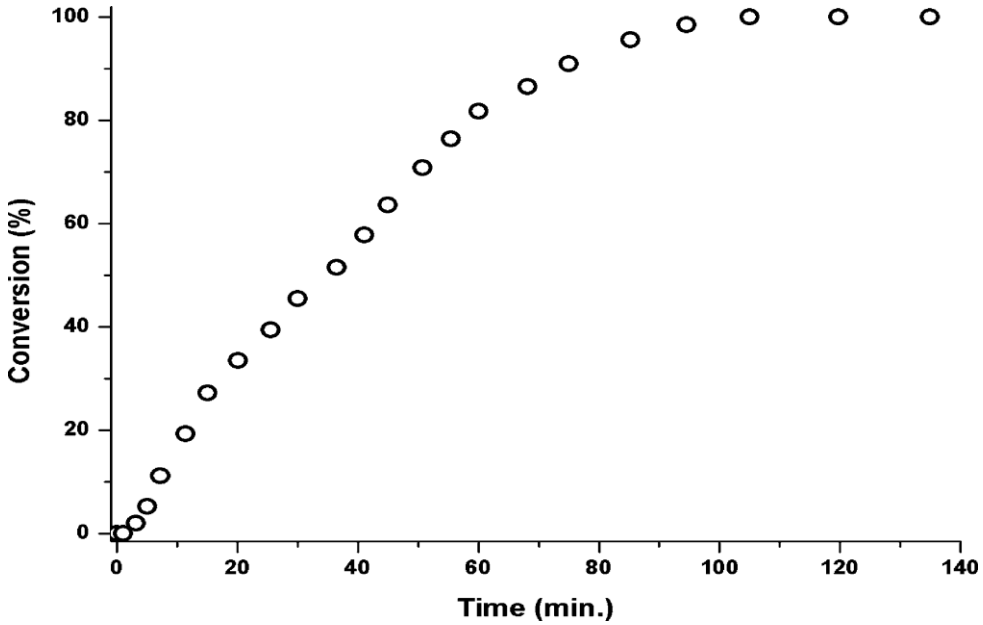

Figure 17. Graph of % conversion *vs.* time for the dehydrogenation of *tert*-butylamine borane starting with 7.5 μmol $[Rh(O_2CC_7H_{15})_2]_2$ and 150 μmol $(CH_3)_3CNH_2BH_3$ in toluene at 25 ± 0.1 ^{0}C.

6.1.1 Characterization of TBAB Dehydrogenation Products

The reaction solution of TBAB dehydrogenation and methanol trap were analyzed by ^{11}B-NMR spectroscopy. The ^{11}B-NMR spectrum of methanol trap shows a resonance at δ = 16.9 ppm (s), **(Figure 18).** This result indicates unambiguously that during the reduction of rhodium(II), the protonation of TBAB leads to the evolution of diborane (B_2H_6) which is trapped in methanol as $B(OMe)_3$ according to the reaction given below [25a]. **(Equation 5)**

$$B_2H_6 + 6CH_3OH \rightarrow 2B(OCH_3)_3 + 6H_2 \quad (5)$$

In addition, ^{11}B NMR spectrum of the reaction medium **(Figure 19)** shows that the concomitant dehydrocoupling of TBAB produces $((CH_3)_3CNH)_2BH$ at δ = 26.9 ppm (d, $J_{B–H}$ = 109 Hz). $((CH_3)_3CNH)_2BH$ is a known product of the dehydrocoupling of *tert*-butylamine borane resulting from metal-mediated B–N bond cleavage and B–H activation [65].

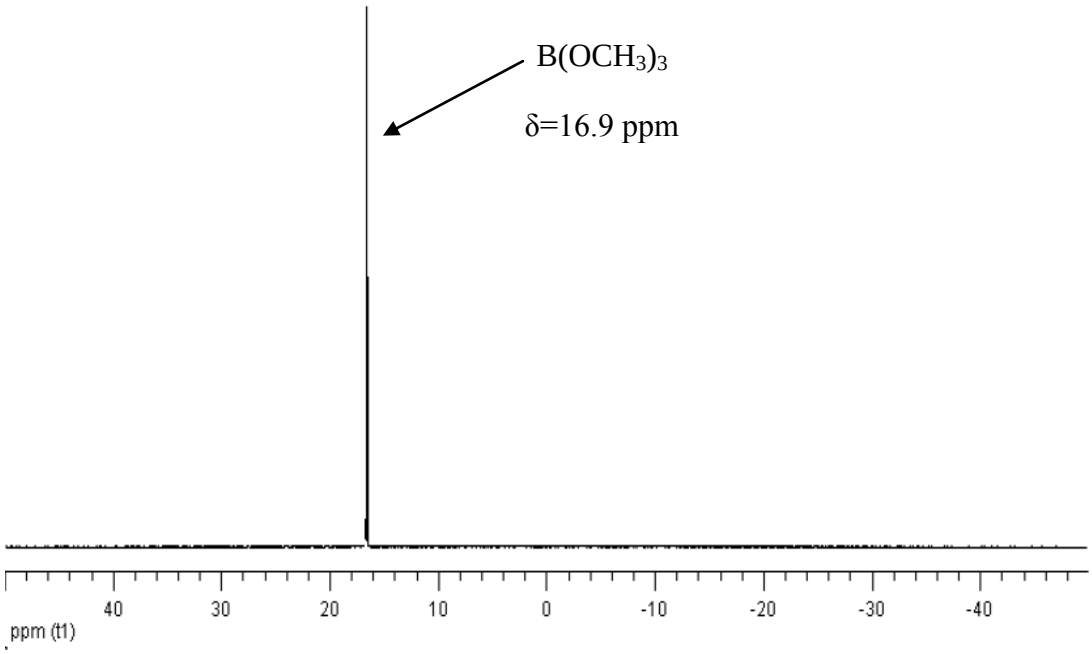

Figure 18. ^{11}B NMR (128.2 MHz, unlocked) spectrum of methanol trap bubbled from the reduction of 7.5 μmol (5.84 mg, 15 μmol of Rh) of $[(CH_3(CH_2)_6CO_2)_2Rh]_2$ in 5 mL of toluene with 150 μmol *tert*-butylamine borane (13.4 mg $(CH_3)_3CNH_2BH_3$).

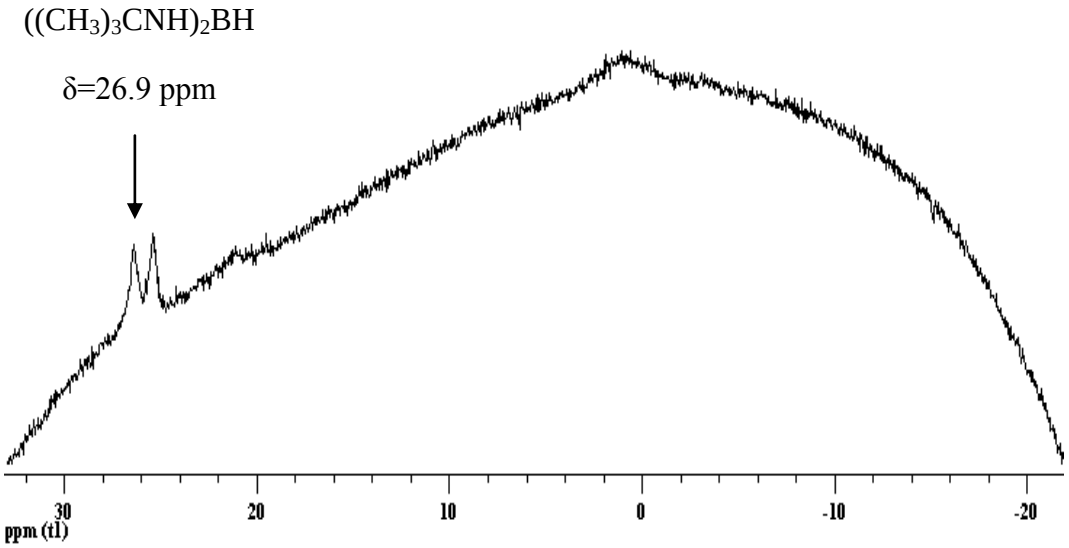

Figure 19. ^{11}B NMR (128.2 MHz, unlocked) spectrum of reaction solution taken at the end of the reduction of 7.5 μmol (5.84 mg, 15 μmol of Rh) of $[(CH_3(CH_2)_6CO_2)_2Rh]_2$ in 5 mL of toluene with 150 μmol *tert*-butylamine borane (13.4 mg $(CH_3)_3CNH_2BH_3$).

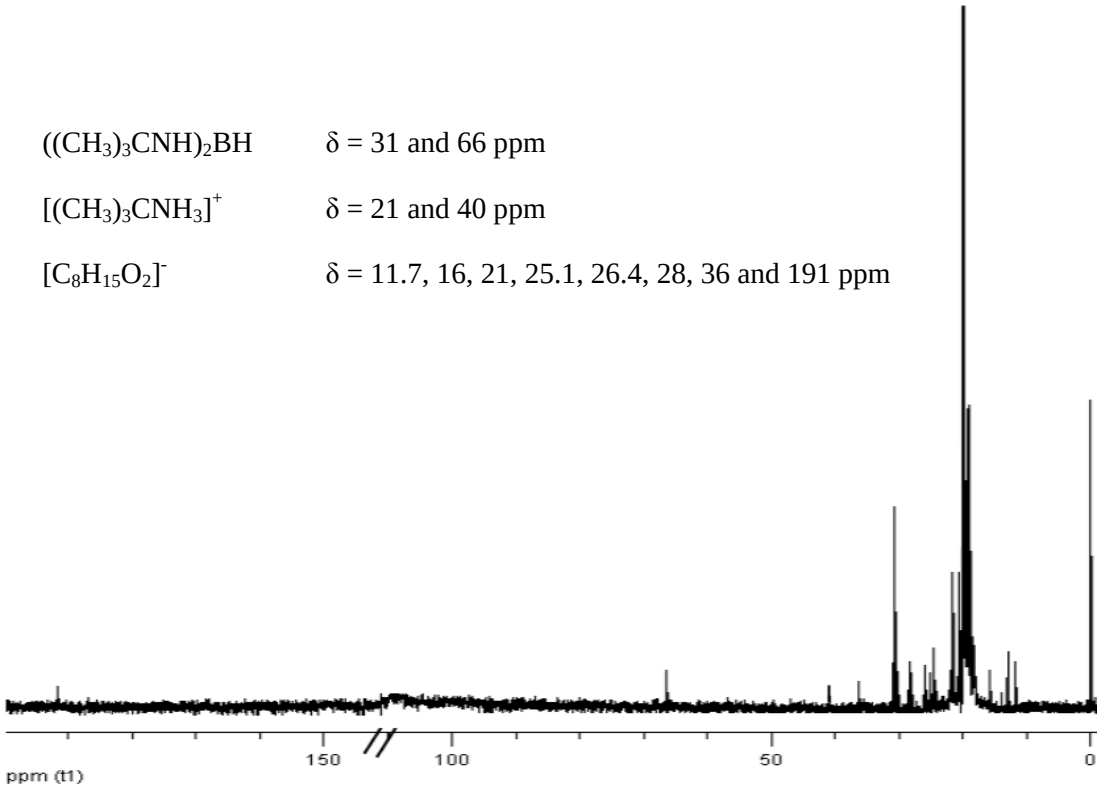

Figure 20. ^{13}C NMR (100.6 MHz, TMS, toluene-d_8) spectrum (solvent peaks in the range of 110-140 ppm were ignored for clarity) taken end of the reduction of 7.5 μmol (5.84 mg, 15 μmol of Rh) of $[(CH_3(CH_2)_6CO_2)_2Rh]_2$ in 5 mL of toluene with 150 μmol *tert*-butylamine borane (13.4 mg $(CH_3)_3CNH_2BH_3$).

The ^{13}C NMR spectrum **(Figure 20)** taken from the reaction solution performed in toluene-d_8 shows only the signals of diamino-borane [$((CH_3)_3CNH)_2BH$] and *tert*-butylammonium octanoate ([$(CH_3)_3CNH_3^+$] [$C_7H_{15}COO^-$]). The formation of $((CH_3)_3CNH)_2BH$, a known product of the dehydrocoupling of *tert*-butylamine borane, is consistent with the B-H activation observed in the dehydrogenation of amine-boranes. The formation of $[(CH_3)_3CNH_3^+][C_7H_{15}COO^-]$ is likely arising from the protonation of *tert*-butylamine borane by octanoic acid, which is generated as transient from the reduction of rhodium(II) octanoate in solution. The signals at δ = 31 and 66 ppm are assigned to the methyl and quaternary carbon atoms of $(CH_3)_3CNH)_2BH$ respectively [66]. The signals at 21 and 40 ppm are ascribed methyl and quaternary carbons of $[(CH_3)_3CNH_3]^+$ respectively. The signals at 11.7, 16, 21, 25.1, 26.4, 28 and 36 ppm

are due to seven carbons in octanoate chain and the signal at 191 ppm to carboxylate carbon of $[C_8H_{15}O_2]^-$ ion [25a].

Figure 21 shows the FTIR spectrum of isolated sample of rhodium(0) nanoparticle powders. The sample gives absorption bands at 1300 and 1390 cm^{-1} for COO^- stretching, 2900–3000 cm^{-1} for C-H stretching in $[C_8H_{15}O_2]^-$ and $[(CH_3)_3CNH_3]^+$, 1000-1250 cm^{-1} for C-N stretching and 3000–3300 cm^{-1} for N–H stretching in $[(CH_3)_3CNH_3]^+$. These results also indicate the presence of octanoate anion and *tert*-butylammonium cation in the environment which are responsible for the stabilization of rhodium(0) nanoparticles [67].

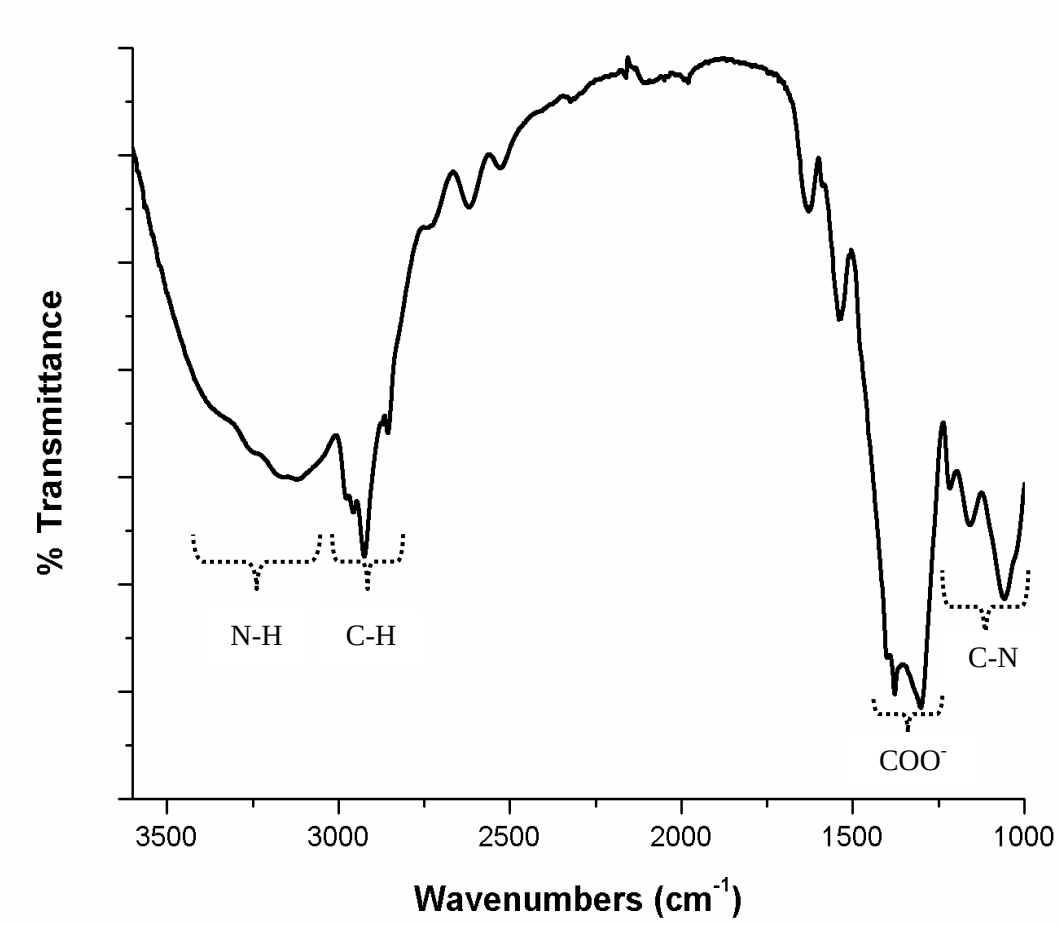

Figure 21. Fourier transformed IR spectrum (taken from KBr pellet in the range of 3600-1000 cm^{-1}) of isolated rhodium(0) nanoparticles.

Furthermore, ICP-OES and elemental analyses of the isolated Rh(0) NPs sample confirm the formation of 1 equiv. of Rh(0) to 2 equiv. of $[(CH_3)_3CNH_3^+][C_7H_{15}COO^-]$. ICP-OES and elemental analyses of Rh(0) NPs sample, calculated (%) for 1 Rh(0) + 2 ($[(CH_3)_3CNH_3][C_8H_{15}O_2]$) as: Rh, 19.2; C, 53.6; H, 10.1; N, 5.2. Found: Rh, 19.1; C, 53.0; H, 9.9; N, 5.1.

Taking all the results together we could establish the stoichiometry for the one-pot synthesis of *tert*-butylammonium octanoate stabilized rhodium(0) nanoparticles from the reduction of rhodium(II) octanoate by *tert*-butylamine borane in toluene at room temperature as follows:

$$[Rh(O_2CC_7H_{15})_2]_2 + 8(CH_3)_3CNH_2BH_3 \xrightarrow{\text{Toluene, RT}} 2/n\ Rh(0)_n + 4[(CH_3)_3CNH_3)]^+[C_7H_{15}CO_2]^- + 3B_2H_6 + 2[((CH_3)_3CNH)_2BH] + 2H_2$$

Additionally, the amount of hydrogen evolved from both the dehydrogenation of *tert*-butylamine borane and methanolysis of diborane was measured to be ~10 mL which is in agreement with the theoretical value expected according to net stoichiometry given above.

6.1.2 Characterization of Rh(0) NPs

The oxidation state, size, composition and morphology of the Rh(0) NPs were investigated by UV-VIS, TEM, STEM, STEM/EDX, XRD and XPS Spectroscopies. During the TBAB reduction of $[Rh(O_2CC_7H_{15})_2]_2$ the reaction solution gradually changes its color from green to dark brown **(Figure 22b)**. This color change reflects the reduction of Rh^{2+} to Rh^0 and provides a convenient way to follow the reaction by UV-VIS electronic absorption spectroscopy. The initial solution of $[Rh(O_2CC_7H_{15})_2]_2$ in toluene exhibits three absorption bands at 306, 427 and 691 nm **(Figure 22a)**; the former band is attributable to the LMCT transition and the latter two to the *d-d* transitions in $[Rh(O_2CC_7H_{15})_2]_2$ [68]**.** UV-VIS spectrum of the final dark brown solution exhibits an absorption continuum, characteristic for rhodium(0) nanoparticles because of the surface plasmon resonance [69].

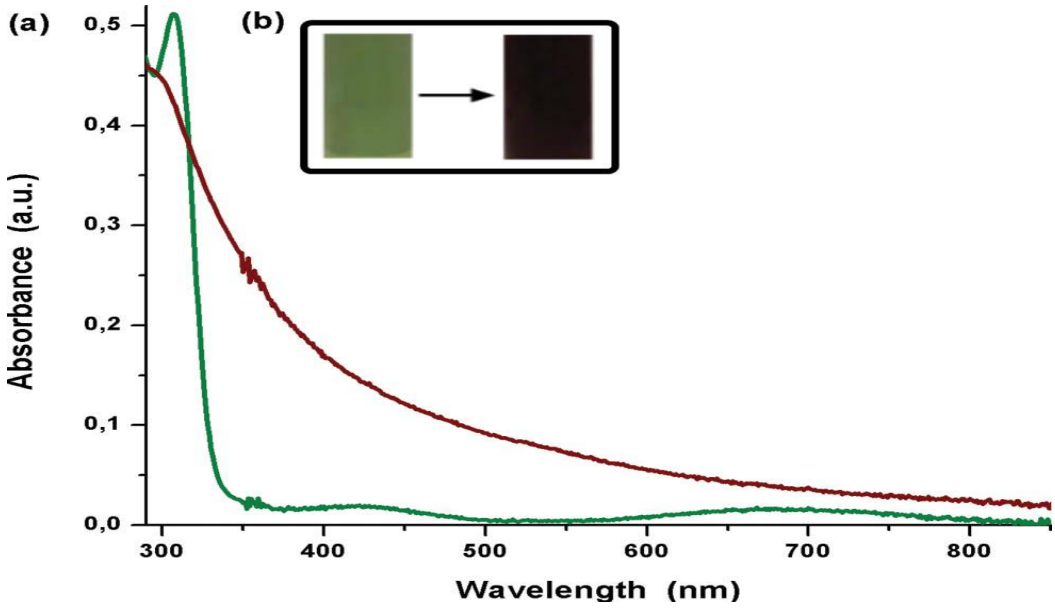

Figure 22. (a) UV-VIS electronic absorption spectra of $[Rh(O_2CC_7H_{15})_2]_2$ (green), Rh(0) NPs (brown) in toluene solution, **(b)** photographs of $[Rh(O_2CC_7H_{15})_2]_2$ (green) and Rh(0) NPs (brown) solutions in toluene.

The XRD and XPS analyses were performed with isolated samples of rhodium(0) nanoparticles. The powder X-ray diffraction pattern of Rh(0) NPs **(Figure 23)** gives a mean Bragg peak at 41^0 corresponding to [111] diffraction for the face-centered-cubic rhodium [70].

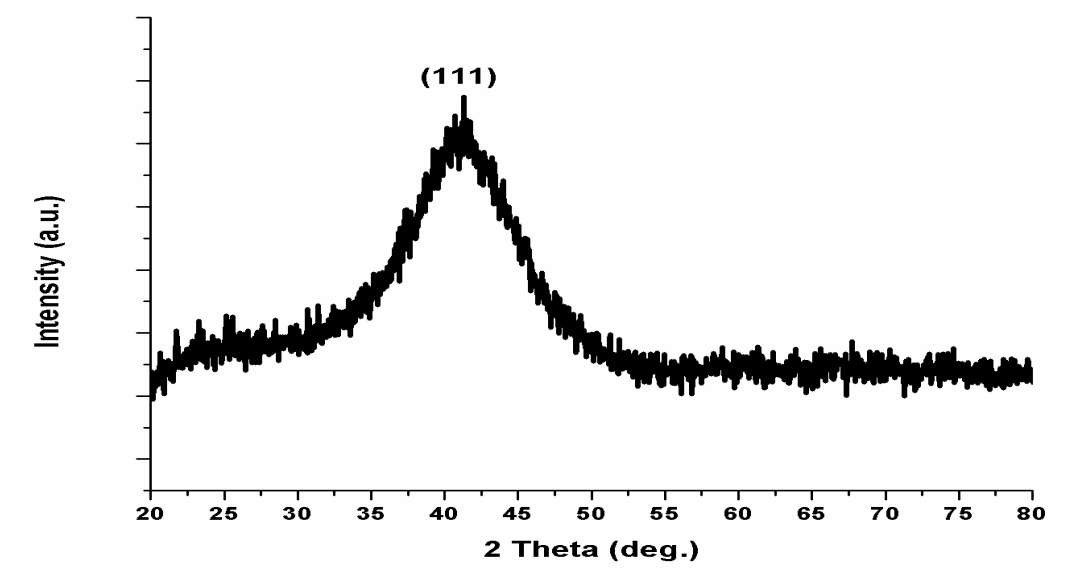

Figure 23. Powder XRD pattern of isolated samples of Rh(0) NPs.

The X-ray photoelectron spectrum of the same sample **(Figure 24)** provides further evidence for the zero oxidation state of rhodium and the surface composition. The high resolution Rh 3d XPS scan **(Figure 24a)** exhibits peaks at 305 and 309 eV, which are readily assigned to Rh(0) $3d_{5/2}$ and Rh(0) $3d_{3/2}$, respectively [71]. In addition to Rh the other main peaks observed in the XPS survey scan **(Figure 24b)** are C 1s, N 1s and O 1s at 285, 402 and 540 eV, respectively.

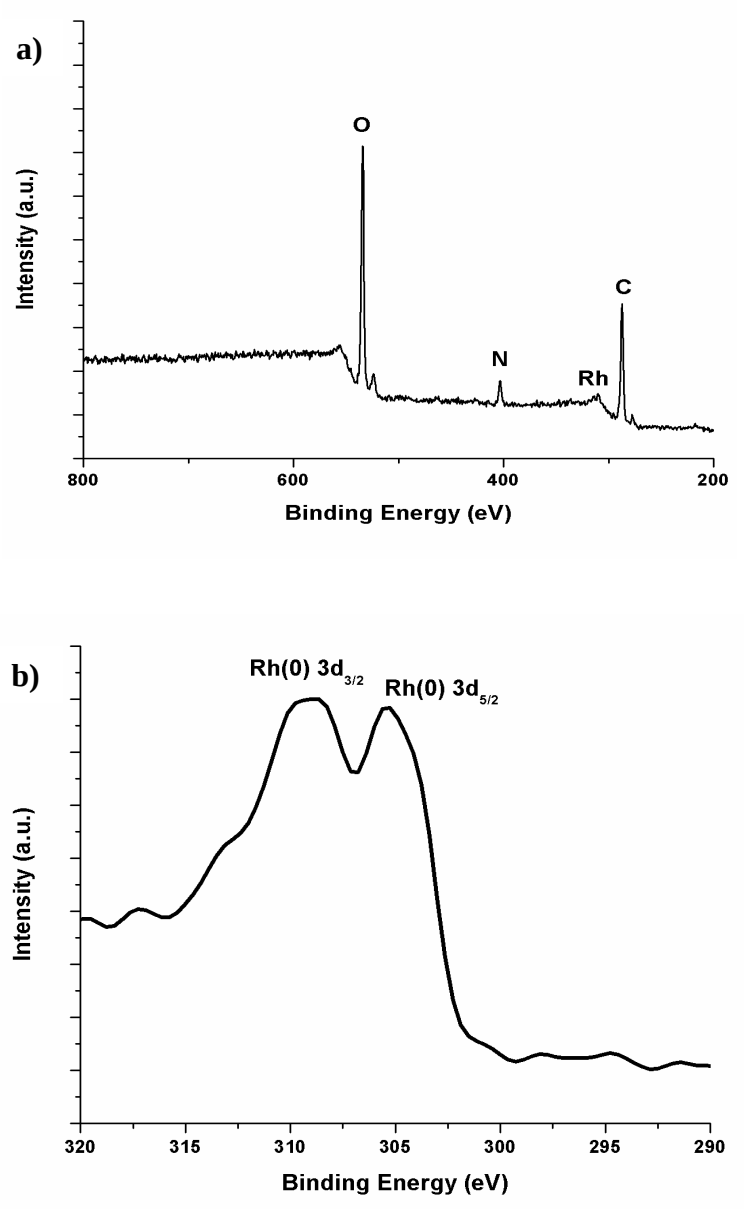

Figure 24. (a) Survey scan, **(b)** High-resolution Rh 3d XPS spectra of isolated Rh(0) NPs.

The size, morphology and composition of Rh(0) NPs were investigated by TEM, STEM, STEM/EDX. TEM studies on the rhodium(0) nanoparticles were started by taking the TEM image of a solution of the precursor complex, $[Rh(O_2CC_7H_{15})_2]_2$, by considering the results of Manners [72] and Finke [73] groups, reporting that the TEM beam induces rhodium(0) nanoparticles formation from $[(1,5\text{-COD})RhCl]_2$ and $[Rh(\eta^5\text{-}C_5Me_5)Cl_2]_2$ precatalysts, respectively.

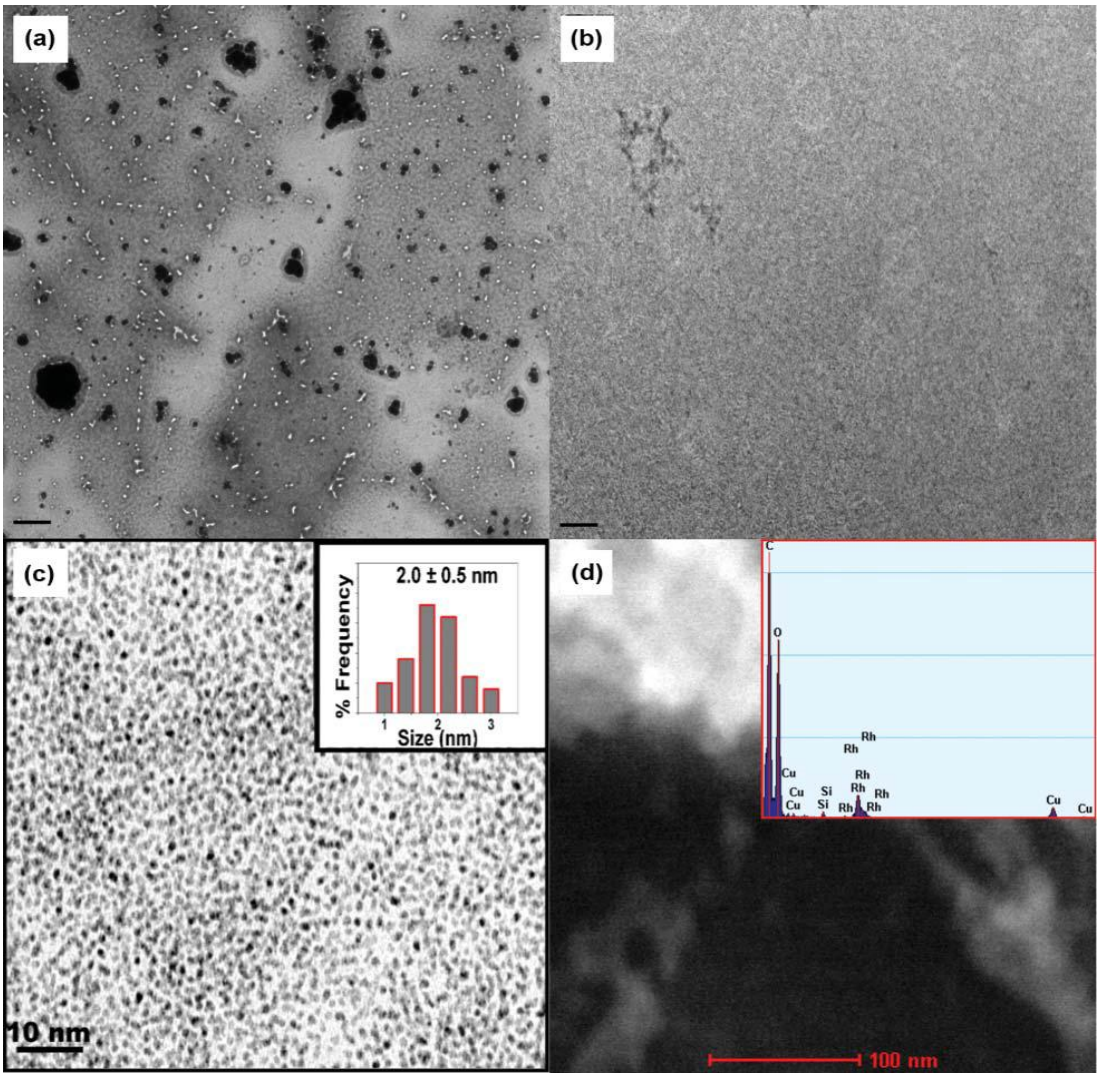

Figure 25. TEM images of **(a)** $[Rh(O_2CC_7H_{15})_2]_2$ in toluene, **(b)** reaction mixture (7.5 μmol $[Rh(O_2CC_7H_{15})_2]_2$ and 150 μmol $(CH_3)_3CNH_2BH_3$ in toluene) harvested after 40 min, **(c)** Rh(0) NPs formed at the end of the dehydrogenation of TBAB, **(d)** STEM image and EDX spectrum of Rh(0) NPs (scale bars in (a) and (b) equal to 2 mm).

A low-resolution TEM image of the $[Rh(O_2CC_7H_{15})_2]_2$ precursor depicts the presence of only micrometre-sized particles **(Figure 25a)**. However, under the same conditions, a low-resolution TEM image of the sample harvested from the solution after 40 min in the dehydrogenation reaction started with TBAB and $[Rh(O_2CC_7H_{15})_2]_2$ in toluene shows only the presence of rhodium(0) nanoparticles **(Figure 25b–c)**. The mean particle size of rhodium(0) nanoparticles was found to be 2.0 ± 0.5 nm corresponding to $Rh(0)_{\sim 300}$ nanoclusters [74] as measured from the TEM image given in **Figure 25c**. The EDX analyses during the STEM observation from many different areas of the same sample also confirm the presence of rhodium in the sample as judged by $L_{\alpha 1}$, $L_{\beta 1}$, L_{b1}, L_{b2}, and L_{g1} lines of Rh at 2.7, 2.8, 2.85, 3.0 and 3.2 keV, respectively **(Figure 25d)**. [75]

Rhodium(0) nanoparticles were found to be highly stable in solution. No precipitation of bulk rhodium(0) from the solution was observed over several months of storage. They could be isolated as a dark brown solid by precipitating out of the colloidal solution upon adding cold hexane, then drying under vacuum (10^{-3} mbar). Rh(0) NPs isolated as a dark brown powder from the reaction solution were found to be redispersible in most common organic solvents such as THF, benzene, toluene, and xylenes. Of particular interest, the TEM image of Rh(0) NPs redispersed in THF **(Figure 26a)** shows the presence of well dispersed Rh(0) NPs with a mean diameter of 2.1 ± 0.4 nm corresponding to $Rh(0)_{\sim 350}$ nanoclusters (histogram in the inset) [74]. The high resolution-TEM image **(Figure 26b)** reveals the highly crystalline feature of these rhodium(0) nanoparticles.

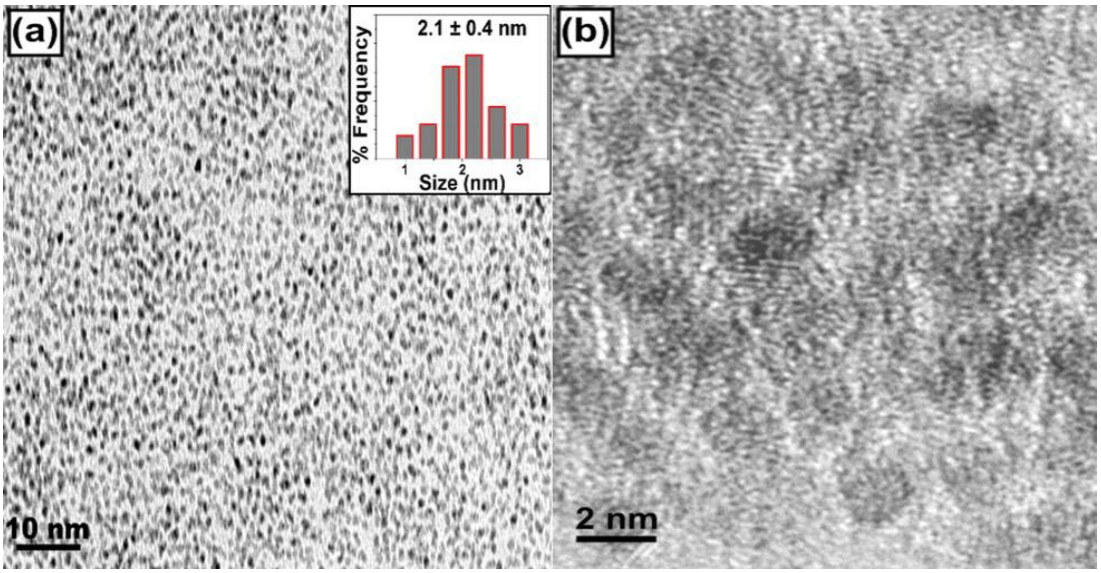

Figure 26. (a) TEM image of Rh(0) NPs isolated and redispersed in THF (scale bar equals to 10 nm) and inset; their size histogram of Rh(0) NPs (≥350 non-touching particles were counted), **(b)** High resolution-TEM image of Rh(0) NPs.

6.2 Catalytic Performance of Rh(0) NPs in the Dehydrogenation of Ammonia Borane

The catalytic activity of Rh(0) NPs was tested in the dehydrogenation of ammonia borane at 25 ^{0}C and determined by measuring the volume of hydrogen gas generated during the reaction. When Rh(0) NPs (15 mM) are added to a THF solution of AB (1.0 M) under argon atmosphere vigorous gas evolution starts immediately with an initial turnover frequency (TOF) of 342 h^{-1} and continues until the release of 1.4 equivalent of H_2 per mol of AB **(Figure 27)**. This *apparent initial* TOF value of 342 h^{-1} provided by Rh(0) NPs is higher than those reported for the prior heterogeneous catalysts [76]. In a control experiment starting with precatalyst $[Rh(O_2CC_7H_{15})_2]_2$ (15 mM Rh) under the same conditions, the dehydrogenation of AB (1.0 M) provides only the release of 0.6 equivalent of H_2 with an initial TOF value of 200 h^{-1} **(Figure 27)** and produces catalytically inactive bulk rhodium(0) metal. The reason of this situation comes from the stronger reducing agent ability of ammonia borane according to *tert*-butylamineborane. The auto-reduction step of ammonia borane is faster than TBAB which leads to the formation of many nanoclusters nuclei that cannot be stabilized by octanoate ion [77].

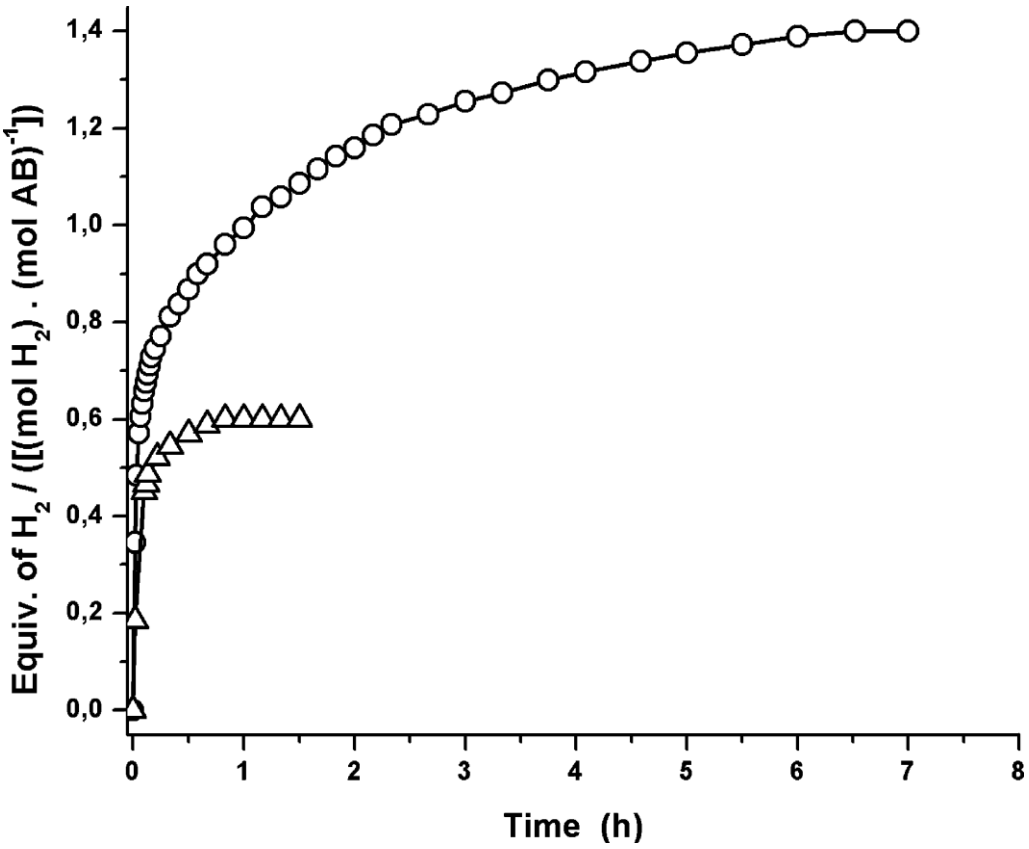

Figure 27. Plot of hydrogen gas evolved per mole ammonia borane *vs.* time observed in two separate experiments for the catalytic dehydrogenation of ammonia borane ($[H_3NBH_3]$ = 1.0 M) in THF at 25.0 ± 0.1 ^{0}C; starting with Rh(0) NPs (circle) and $[Rh(O_2CC_7H_{15})_2]_2$ (triangle) (in both [Rh] = 15 mM).

The reaction products were identified by ^{11}B-NMR Spectroscopy. ^{11}B-{^{1}H} NMR spectra taken from the reaction solution are depicted in **Figure 28**. Once 1.4 equivalent of H_2 is released, the spectrum shows that AB is completely consumed and the spectrum contains only signals for the THF-soluble dehydrogenation products; the broad signals in the range of 0 and -13.4 ppm for singly dehydrogenated boron atoms [17**]** of the cyclic intermediates [13,78] which further partially dehydrogenate to form polyborazylene as evidenced by two resonances centered at 25 and 26 ppm, characteristics for the cross linked B=N (18–40 ppm). [13,17 ,65]

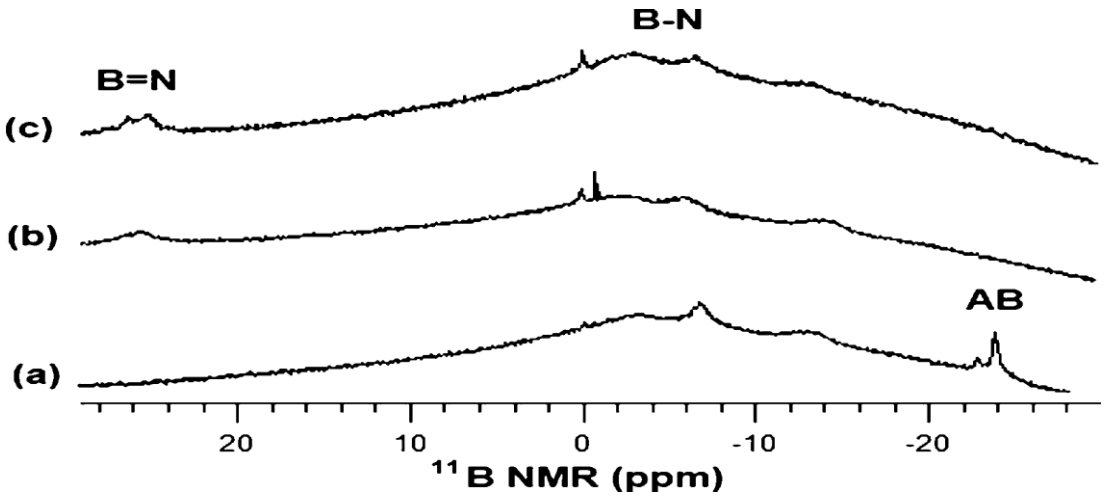

Figure 28. ^{11}B -{^{1}H} NMR spectra of the reaction solution (1.0 M H_3NBH_3 + 15 mM Rh(0) NPs) in THF at 25.0 ± 0.1 ◦C after (a) 15 min, (b) 120 min, (c) 420 min. The broad appearance of each spectrum (in the range of +20 to -20 ppm) resulting from the NMR probe that contains boron.

Additionally, ATR-IR spectrum of the precipitate harvested from the solution after reaction **(Figure 29)** shows the characteristics bands at 3296-3247 cm^{-1} for N-H and 2388-2313 cm^{-1} for B–H of $[H_2NBH_2]_n$ [23**]** which is presumably formed from the subsequent polymerization of singly dehydrogenated cyclic intermediate.

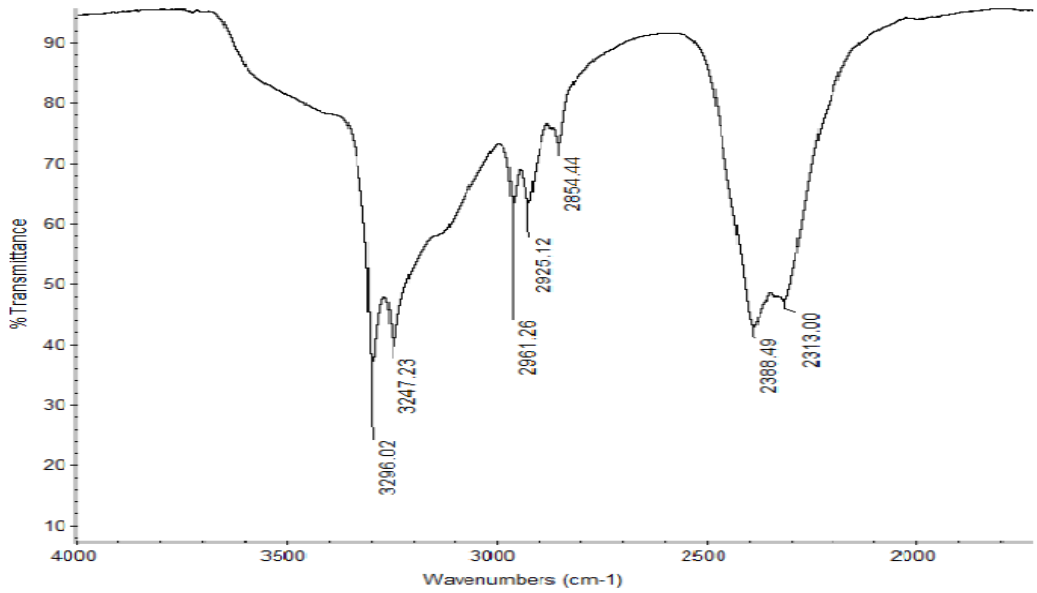

Figure 29. ATR-IR spectrum of the precipitate isolated at the end of the Rh(0) NPs catalyzed dehydrogenation of ammonia borane in THF at 25 ± 0.1 °C.

The ability of mercury(0) to poison heterogeneous metal(0) catalysts, by amalgamating the metal catalyst or being adsorbed on its surface, has been known for a long time; [79**]** this is the single most widely used test of homogeneous *versus* heterogeneous catalysis [80]. The suppression of catalysis upon addition of mercury(0) into the solution is considered to be compelling evidence for heterogeneous catalysis. In this manner, poisoning experiments with mercury(0) were performed to see whether mercury(0) affects the reaction rate or not. Our reaction was entirely ceased by adding 200 eq. of Hg(0) per Rh which indicates that Rh(0) NPs act as a heterogeneous catalyst **(Figure 30)**.

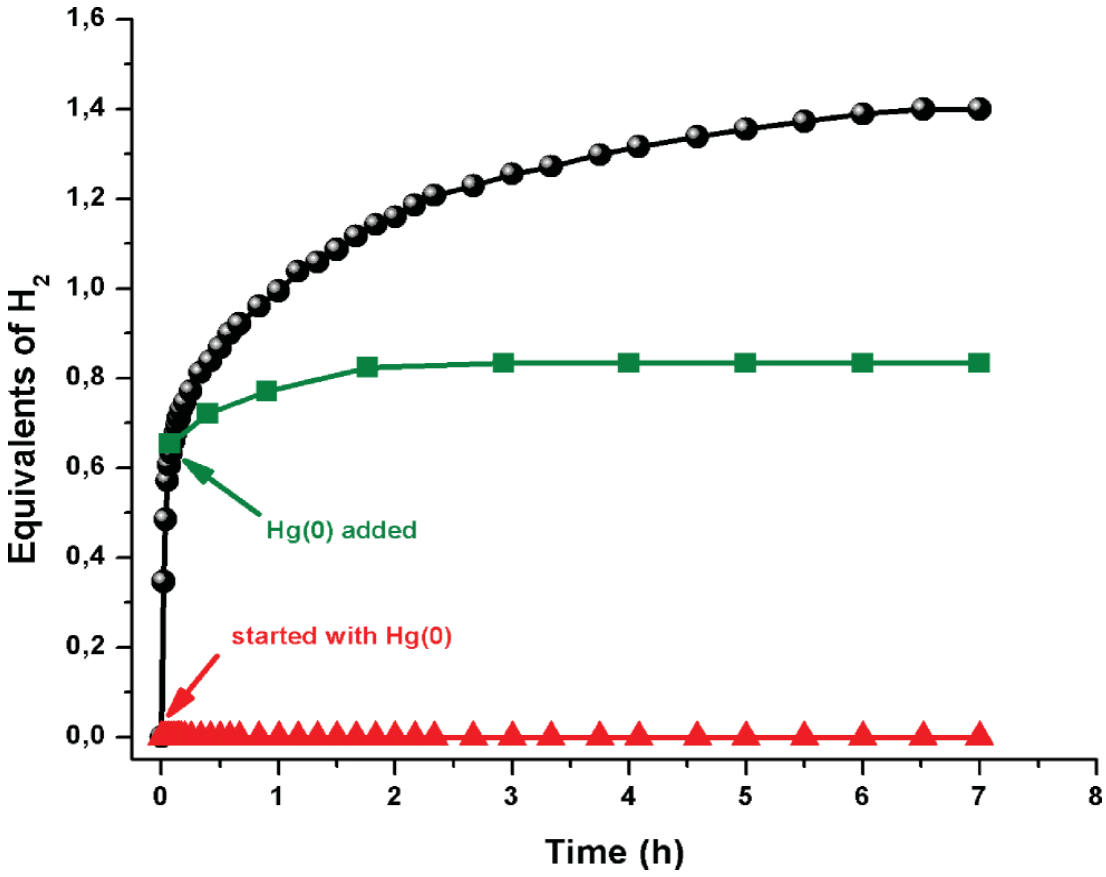

Figure 30. Plot of equivalents of H_2 generated per mole of ammonia borane *vs.* time for Hg(0) poisoning experiments starting with [H_3NBH_3] = 1.0M and [Rh(0) NPs] = 15 mM in THF at 25.0 ± 0.1 ^{0}C; (a) in the absence of Hg(0) (black spheres ●), (b) after the addition of 200 equiv. of Hg(0) (0.3 g, 1.5 mmol) when 45% of conversion achieved (green squares ■), (c) starting with 200 equiv. of Hg(0) (0.3 g, 1.5 mmol) (red triangles ▲).

Rh(0) NPs were also tested for their lifetime, and reusability as a heterogeneous catalyst in the dehydrogenation of AB at room temperature. A catalyst lifetime experiment was performed starting with 2.5 mM Rh(0) NPs and 5 M AB at 25 ± 0.1 ^{0}C. Rh(0) NPs provide 1100 turnovers over 72 h before deactivation by aggregation into catalytically inactive bulk rhodium. In order to test the reusability of Rh(0) NPs, they were precipitated out as a dark brown powder by adding cold hexane under Ar atmosphere. Such isolated Rh(0) NPs were found to be readily redispersible in THF and yet an active catalyst in dehydrogenation of AB.

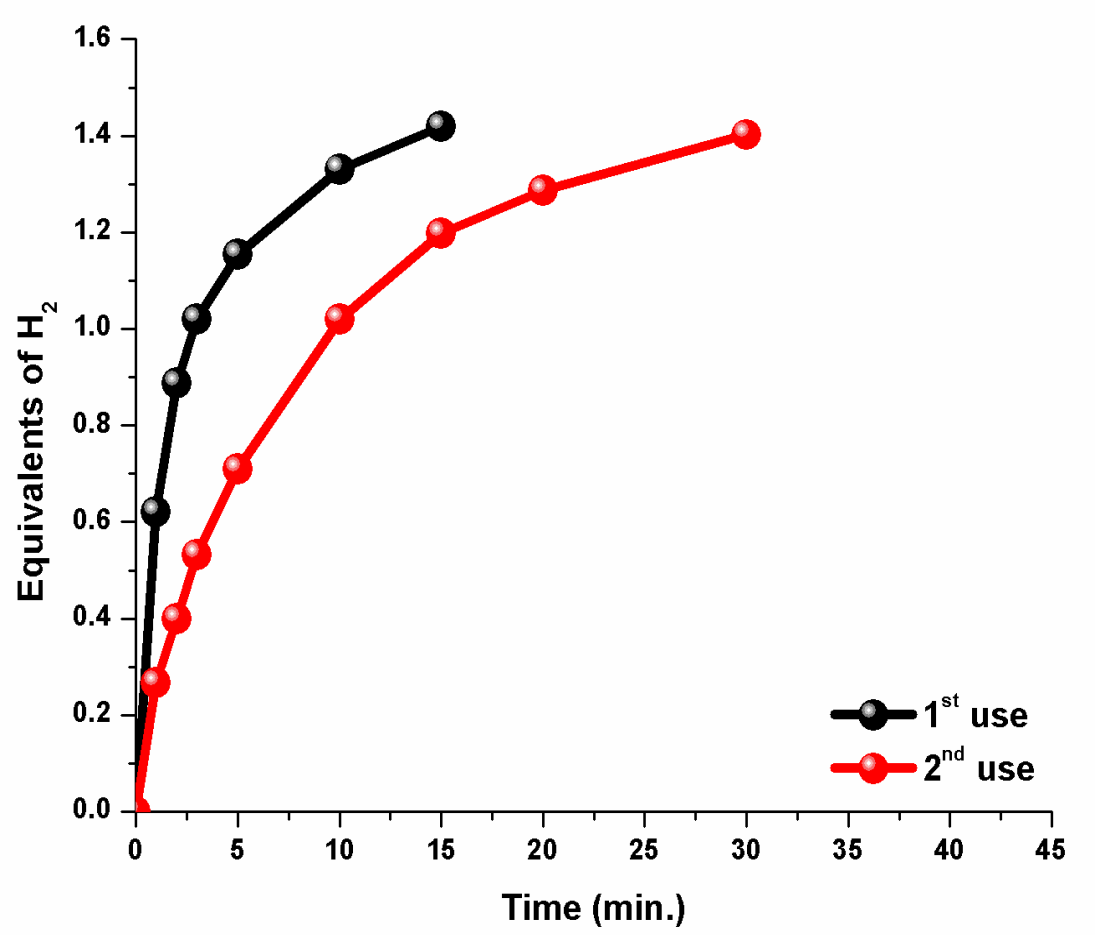

Figure 31. Equivalents of H_2 vs time graph for **(a)** 30 mM Rh(0) NPs catalyzed dehydrogenation of 150 mM ammonia borane in THF at 25 ± 0.1 °C (black), **(b)** the isolated Rh(0) NPs (from the first run) catalyzed dehydrogenation of ammonia borane (red) under the same conditions in the first run.

They retain 60% of their initial catalytic activity [81] in the second run with complete conversion of AB and generation of the same amount of H_2 under the same conditions as in the first run **(Figure 31)**. The 40% decrease in the catalytic activity observed in the second run may be attributed to the fall in the number of active surface atoms due to the increase of the size of rhodium(0) nanoparticles by agglomeration. Indeed, a TEM image of Rh(0) NPs after the first run of dehydrogenation **(Figure 32)** shows an increase in the average size to 2.9 ± 0.5 nm, corresponding to $Rh(0)_{\sim 930}$ nanoclusters [74].

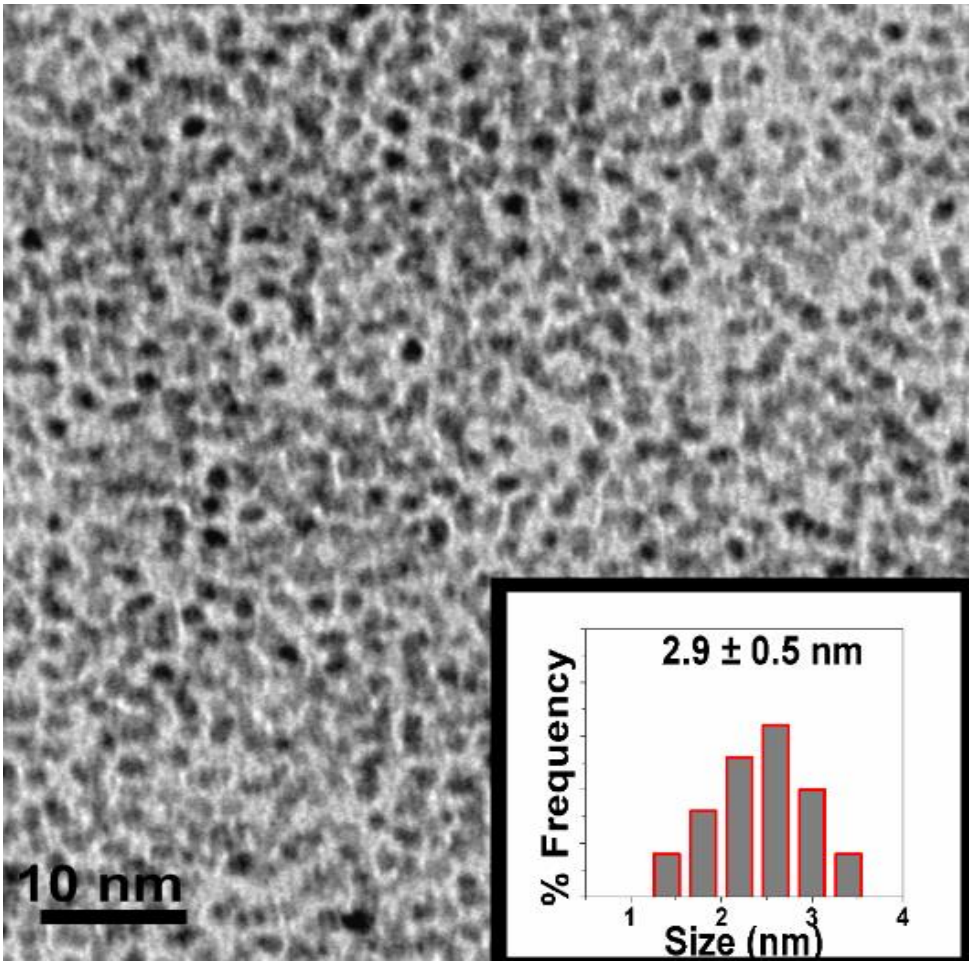

Figure 32. TEM image and corresponding size histogram of Rh(0) NPs harvested after the dehydrogenation of ammonia borane in THF at 25 ± 0.1 ^{0}C.

CHAPTER 7

CONCLUSIONS

To conclude, the main findings of my dissertation on the preparation and characterization *tert*-butylammonium octanoate stabilized rhodium(0) nanoparticles as catalyst for the dehydrogenation of ammonia borane can be summarized as follows:

- For the first time, *tert*-butylammonium octanoate stabilized rhodium(0) nanoparticles were reproducibly prepared by the *tert*-butylamine borane reduction of rhodium(II) octanoate dimer at room temperature.

- The characterization of this novel catalyst system by ICP-OES, TEM, STEM, EDX, XRD, XPS, FTIR, UV-VIS, and ^{1}H, ^{13}C, and ^{11}B NMR spectroscopic methods and elemental analysis reveals that octanoate anions and *tert*-butylammonium cations take part in the stabilization of rhodium(0) nanoparticles.

- These *tert*-butylammonium octanoate stabilized rhodium(0) nanoparticles are found to be highly stable. No precipitation of bulk rhodium(0) from the solution was observed over after several months of storage, demonstrating the efficiency of *tert*-butylammonium octanoate in the stabilization of rhodium(0) nanoparticles.

- The Rh(0) NPs show unprecedented catalytic activity among all heterogeneous catalysts tested in the dehydrogenation of ammonia borane even at room temperature by providing a release of 1.4 equivalent H_2 and

generation of polymeric B–N and B=N species with an *apparent initial* TOF value of 342 h^{-1} and TTO value of 1100.

- The dehydrogenation of ammonia borane is also achieved even in the second successive run performed by redispersing the Rh(0) NPs isolated after the first run, whereby Rh(0) NPs retain 60% of their initial catalytic activity with complete conversion of ammonia borane and generation of the same amount of H_2 under the same conditions as in the first run. Although a significant portion of the inherent catalytic activity has been lost in the second run, Rh(0) NPs are the first example of an isolable and reusable nanoparticles catalyst employed in this important reaction.

REFERENCES

[1] (a) Polshettiwar, V., Varma, S. R., *Green. Chem*., **2010**, 12, 743 (b) Schögl, R., Abd Hamid, S. B., *Angew. Chem. Int. Ed.*, **2004**, 43, 1628

[2] Yan, N., Xiao, C., Kou, Y., *Coord. Chem. Rev*., **2010**, 254, 1179

[3] Armoli, N., Balzani, V., *ChemSusChem*, **2011**, 4, 21

[4] Balat, M., *Int. J. Hydrogen Energy*, **2008**, 33, 4013

[5] See Figure 14 at page 26.

[6] Basic Research Needs Catalysis for Energy, Report from the US Department of Energy, Basic Energy Sciences Workshop Report, August 6–8, **2007**, http://www.sc.doe.gov/bes/reports/list.html

[7] (a) Wolf, G., Baumann, J., Baitalow, F., Hoffmann, F. P., *Thermochim. Acta*, **2000**, 343, 19 (b) Gutowska, A., Li, L., Shin, Y., Wang, C. M., Li, X. S., Linehan J. C., et. al., *Angew. Chem., Int. Ed.*, **2005**, 44, 3578 (c) He, T., Xiong, Z., Wu, G., Chu, H., Wu, C., Zhang T., Chen, P., *Chem. Mater.*, **2009,** 21, 2315

[8] (a) Zahmakıran, M., Durap, F., Özkar, S., *Int. J.Hydrogen Energy*, **2010**, 35, 187 (b) Zahmakıran, M., Özkar, S., *Appl. Catal., B*, **2009**, 89, 104 (c) Durap, F., Zahmakıran, M., Özkar, S., *Appl. Catal., A*, **2009**, 369, 53 (d) Staubitz, A., Robertson, A. P. M., Manners, I., *Chem. Rev.*, **2010**, 110, 4079 (e) Bluhm, M. E., Bradley, M. G., Butterick, R., Kusari, U., Sneddon, L. G., *J. Am. Chem. Soc.*, **2006**, 128, 7748 (f) Himmelberger, L. R., Bluhm, M. E., Sneddon, L. G., *Inorg. Chem.*, **2009**, 48, 9883 (g) Stephens, F. H., Baker, R.

T., Matus, M. H., Grant D. J., Dixon, D. A., *Angew. Chem., Int. Ed.*, **2007**, 46, 746 (h) Miller, A. J. M., Bercaw, J. E., *Chem. Commun.*, **2010**, 46, 1709

[9] Smythe, N. C., Gordon, J. C., *Eur. J. Inorg. Chem.*, **2010**, 509

[10] (a) Davis, B. L., Dixon, D. A., Garner, E. B., Gordon, J. C., Matus, M. H., Scott, B., Stephens, F. H., *Angew. Chem. Int. Ed.*, **2009**, 48, 6812. (b) Mock, M. T., Potter, R. G., Camaioni, D. M., Li, J., Dougherty, W. G., Kassel, W.S., et. al. *J. Am. Chem. Soc.*, **2009**, 131, 14454 (c) Sutton A. *et al.* US Patent Application 12/762895, **2010**, *cf.* http://ip.com/patapp/US20100272622

[11] (a) Jaska, C. A., Temple, K., Lough, A. J., Manners, I., *Chem. Commun.*, **2001**, 962 (b) Jaska, C. A., Temple, K., Lough, A. J., Manners, I., *J. Am. Chem. Soc.*, **2003**, 125, 9424

[12] Rousseau, R., Schenter, G. K., Julton, J. L., Linehan, J. C., Engelhard, M. H., Autrey, T., *J. Am. Chem. Soc.*, **2009**, 131, 10516

[13] Shrestha, R. P., Diyabalanage, H. V. K., Semelsberger, T. A., Ottand, K. C., Burrell, A. K., *Int. J. Hydrogen Energy*, **2009**, 34, 2616

[14] (a) Clark, T. J., Russell, C. A., Manners, I., *J. Am. Chem. Soc.*, **2006**, 128, 9582 (b) Fulton, J. L., Linehan, J. C., Autrey, T., Balasubramanian, M., Chen, Y., Szymczak, N. K., *J. Am. Chem. Soc.*, **2007**, 129, 11936 (c) Jiang, Y., Berke, H., *Chem. Commun.*, **2007**, 3751 (d) Paul A., Musgrave, C. B., *Angew. Chem., Int. Ed.*, **2007**, 46, 8153 (e) Douglas, T. M., Chaplin, A. B., Weller, A. S., *J. Am. Chem. Soc.*, **2008**, 130, 14432 (f) Staubitz, A., Soto, A. P., Manners, I., *Angew. Chem. Int. Ed.*, **2008**, 47, 6212 (g) Yang, X., Hall, M. B., *J. Am. Chem. Soc.*, **2008**, 130, 1798 (h) Forster, T. D., Tuononen, H. M., Parvez, M., Roesler, R., *J. Am. Chem. Soc.*, **2009**, 131, 6689 (i) Kawano,

Y., Uruichi, M., Shiomi, M., Taki, S., Kawaguchi, T., Kakizawa, T., Ogino, H., *J. Am. Chem. Soc.*, **2009**, 131, 14946

[15] See this wonderful paper and the references therein. Watzky, M. A., Finke, R. G., *J. Am. Chem. Soc.* **1997,** 119, 10382

[16] Denney, M. C., Pons, V., Hebden, T. J., Heinekey, D. M., Goldberg, K. I., *J. Am. Chem. Soc.*, **2006**, 128, 12048

[17] Keaton, R. J., Blacquiere, J. M., Baker, R. T., *J. Am. Chem. Soc.*, **2007**, 129, 184

[18] Pun, D., Lobkovsky, E., Chirik, P. J., *Chem. Commun.*, **2007**, 3297

[19] Blacquiere, N., Diallo-Garcia, S., Gorelsky, S. I., Black, D. A., Fagnou, K., *J. Am. Chem. Soc.*, **2008**, 130, 14034.

[20] Alcaraz, G., Vendier, L., Clot, E., Sabo-Etienne, S., *Angew. Chem. Int. Ed.*, **2010**, 49, 918

[21] Conley, B. L., Williams, T. J., *Chem. Commun.*, **2010**, 46, 4815

[22] Kim, S. K., Han, W. S., Kim, T. J., Kim, T. Y., Nam, S. W., Mitoraj, M., et. al., *J. Am. Chem. Soc.*, **2010**, 132, 9954

[23] Staubitz, A., Sloan, M. E., Robertson, A. P. M., Friedrich, A., Schneider, S., Gates, P. J., Gunne J. S., Manners, I., *J. Am. Chem. Soc.*, **2010**, 132, 13332

[24] See Chapter 2.

[25] (a) Zahmakıran, M., Özkar, S., *Inorg. Chem.*, **2009**, 48, 8955 (b) Zahmakıran, M., Tristany, M., Philippot, K., Fajerwerg, K., Özkar, S., Chaudret, B., *Chem. Commun.*, **2010**, 46, 2938

[26] Oyama, S. T., Somorjai, G. A., *J. Chem. Educ.*, **1986**, 65, 765

[27] Fogler, H. S., Gürmen, M. N., *Elements of Chemical Reaction Engineering*, Upper Saddle River, N.J. : Prentice Hall PTR, **1999**

[28] Hagen, J., *Industrial Catalysis: A Practical Approach*, Wiley-VCH, Mannheim, Germany, **2006**

[29] Astruc, D., *Nanoparticles and Catalysis*, Wiley-VCH Verlag GmbH & Co. KGaA, Weinheim, **2008**

[30] Anastas, P. T., Warner, J. C., *Green Chemistry: Theory and Practice*, Oxford University Press: New York, **1998**

[31] (a) Astruc, D., Lu, F., Aranzaes, J.R., *Angew. Chem. Int. Ed.* **2005**, *44*, 7399 (b) De Vries, J. G., *Dalton Trans.* **2006**, 3, 421

[32] Fahlman, B. D., *Materials Chemistry*, Springer: Mount Pleasant, MI, **2007**, Vol. 1

[33] Waychunas, G. A., *Rev. Mineral. Geochem.*, **2001**, 44, 105

[34] Feldheim, D. L., Foss, Jr., C. A., *Metal Nanoparticles: Synthesis, Characterization and Applications*, Marcel Dekker Inc., Basel, Switzerland. **2002**

[35] Corain, B., Schmid, G., Toshima, N., *Metal Nanoclusters in Catalysis and Materials Science: The Issue of Size Control*, Elsevier B.V., Amsterdam, Netherlands, **2008**, and the references in Chapter 2 and 4

[36] Castro, T., Reifenberger, R., Choi, E., Andres, R. P., *Phys. Rev. B*, **1990**, 13, 8548

[37] Mie, G., *Ann. Phys*., **1908**, 25, 377

[38] Simon, U., Schön, G., Schmid, G., *Angew. Chem. Int. Ed. Engl*., **1993**, 32, 250

[39] Glanz, J., *Science*, **1995**, 269, 1363

[40] Elghanian, R., Storhoff, J. J., Mucic, R. C., Letsinger, R. L., Mirkin, C. A., *Science*, **1997**, 277, 1078

[41] Colvin, V. L., Schlamp, M. C., Alivisatos, A. P., *Nature*, **1994**., 370, 354

[42] Reetz, M. T., Winter, M., Dumpich, G., Lohau, J., Friedrichowski, S., *J. Am. Chem. Soc.* **1997**, 119, 4539

[43] Zahmakıran, M., Tonbul, Y., Özkar, S., *Chem. Comm*., **2010**, 46, 4788

[44] Stein, J., Lewis, L. N., Gao, Y., Scott, R. A., *J. Am.Chem. Soc*., **1999**, 121, 3693

[45] Reetz, M. T., Quaiser, S. A., Merk, C., *Chem. Ber*., **1996**, 129, 741

[46] (a) Durap, F., Metin, Ö., Aydemir, M., Özkar, S., *Appl. Organometal. Chem.* **2009**, 23, 498 (b) Metin, Ö., *Doktorate Thesis: Synthesis and Characterization of Water Soluble Polymer Stabilized Transition Metal(0) Nanoclusters as Catalyst in Hydrogen Generation From the Hydrolysis of Sodium Borohydride and Ammonia Borane*, METU, **2010**

[47] (a) Pachon, L. D., Rothenberg G., *Appl. Organometal. Chem*., **2008**, 22, 288 (b) Aiken, J. D., Finke, R. G., *J. Mol. Cat. A.: Chem*., **1999**, 145, 1 (c) Özkar, S., Finke, R. G., *J. Am. Chem. Soc*., **2002**, 124, 5796

[48] Schmid, G., *Nanoparticles: From Theory to Application*, Viley-VCH, Weinheim, **2010**

[49] Bayram, E., Zahmakıran, M., Özkar, S., Finke, R. G., *Langmuir*, **2010**, 26, 12455

[50] Ayvalı, T., Zahmakıran, M., Özkar, S., *Dalton Trans*., **2011**, 40, 3584

[51] Erdogan, H., Metin, Ö., Özkar, S., *Phys. Chem. Chem. Phys.*, **2009**, 11, 10519

[52] (a) Reetz, M. T., Helbig, W., Quaiser, S. A., Stimming, U., Breuer, N., Vogel, R., *Science*, **1995**, 267, 367 (b) Reetz, M. T., Breinbauer, R., Wanninger, K., *Tetrahedron Lett*., **1996**, 37, 4499

[53] Zhao, M., Sun, L., Crooks, R. M., *J. Am. Chem. Soc*., **1998**, 120, 4877

[54] Lin, Y., Finke, R. G., *J. Am Chem. Soc*. **1994**, 116, 8335

[55] (a) Metin, Ö., Özkar, S., Sun, S. H., *Nano. Res.*, **2010**, 3, 676 (b) Sayle, D. C., Doig, J. A., Parker, S. C, Watson, G. W., *J. Mater. Chem*., **2003**, 13, 2078

[56] (a) Zahmakıran, M., Akbayrak, S., Kodaira, T., Özkar, S., *Dalton Trans*., **2010**, 39, 7521 (b) Zahmakıran, M., Tonbul, Y., Özkar, S., *J. Am. Chem. Soc*., **2010**, 132, 6521

[57] El-Shall, M. S., Abdelsayed, V., Khder, A. E. R. S., Hassan, H. M. A., El-Kaderi, H. M., Reich, T. E., *J. Mater. Chem*., **2009**, 19, 7625

[58] Reetz, M. T., Helbig, W., *J. Am. Chem. Soc*., **1994**, 116, 7401

[59] Turkevich, J., Stevenson, P. C., Hillier, J., *Discuss. Faraday Soc*., **1951**, 11, 55

[60] Bönnemann, H., Richards, R., *Eur. J. Inorg. Chem*., **2001**, 2455

[61] Hamilton, C. W., Baker, R. T., Staubitz, A., Manners, I., *Chem. Soc. Rev*., **2009**, 38, 279

[62] Felderhoff, M., Weidenthaler, C., von Helmoth, R., Eberle, U., *Phys. Chem. Chem. Phys.*, **2007**, 9, 2643

[63] Nijkamp, M. G., Raaymakers, J. E. M. J., Van Dillen, A. J., De Jong, K. P., *Appl. Phys. A*, **2001**, 72, 619

[64] Chae, H. K., Siberio-Perez, D. Y., Kim, J., Go, Y. B., Eddaoudi, M., Matzger, A. J., et al. *Nature*, **2004**, 427, 523

[65] Pons, V., Baker, R. T., Szymczak, N. T., Heldebrant, D. J., Linehan, J. C., Matus, M. H., et. al., *Chem. Commun.*, **2008**, 6597

[66] (a) Manders, L., Kristen, M. O., Hanschild, A., Geprogs, M., USA Patent, Patent No: US 2001/0007009, **2001** (b) Shastin, A. V., Godovikova, T. I., Korsunsldi, B. L., *Chem. Heterocycl. Compd.*, **1999**, 35, 75

[67] (a) Umumera, J., Cameron, D. G., Manstch, H. H., *J. Phys. Chem.*, **1980**, 84, 2272 (b) Murphy, C. A., Cameron, T. S., Cooke, M. W., Aquino, M. A. S., *Inorg. Chim. Acta*, **2000**, 305, 225

[68] Stranger, R., Medley, A. G., McGrady, J. E., Garrett, J. M., Appleton, T. G., *Inorg. Chem.*, **1996**, 35, 2268

[69] Creighton, J. A., Eadon, D. G., *J. Chem. Soc. Faraday Trans.*, **1991**, 87, 3881

[70] Bruss, J. A., Gelesky, M. A., Machado, G., Dupont, J., *J. Mol. Catal. A: Chem.*, **2006**, 252, 212

[71] (a) Wagner, C., Riggs, W. M., Davis, L. E., Moulder, J. F., Muilenberg, G. E., *Handbook of X-Ray Photoelectron Spoectroscopy*, Perkin–Elmer, **1979**, 55, 3440 (b) Zhang, X., Chan, K. Y., *Chem. Mater.*, **2003,** 15, 451 (c) The reduction of Rh(II) to its zerovalent state was monitored by UV-VIS electronic absorption spectroscopy and to be sure about all Rh(II) reduced to Rh(0), a molar ratio of [TBAB]/[Rh] = 10 was used ; therefore, we did not need to do curve fitting for high resolution Rh 3d XPS spectrum of Rh(0) NPs. However in order to be sure about the absence of Rh(II) in the environment, curve fitting can be done.

[72] Jaska, C. A., Manners, I., *J. Am. Chem. Soc.*, **2004**, 126, 9776

[73] Hagen, C. M., Widegren, J. A., Maitlis, P. M., Finke, R. G., *J. Am. Chem. Soc.*, **2005**, 127, 4423

[74] The numbers of metal atoms (N); $N = N_0\rho V/102.9$, where $N_0 = 6.022 \times 10^{23}$, $\rho = 12.5$ g cm^{-3} and $V = (4/3)\pi(D/2)^3$, D is the diameter.

[75] Jones, I. P., *Chemical Microanalysis Using Electron Beams*, The Institute of Materials, London, **1992**.

[76] See Table 1 given at page 3 of this dissertation.

[77] Zheng, N., Fan, J., Stucky, G. D., *J. Am. Chem. Soc.*, **2006**, 128, 6550

[78] Komm, R., Geanangel, R. A., Liepins, R., *Inorg. Chem.*, **1983**, 22, 1684

[79] Whitesides, G. M., Hackett, M., Brainard, R. L., Lavalleye, J. P., Sowinski, A. F., Izumi, A. N., Moore, S. S., Brown, D. W., Staudt, E. M., *Organometallics*, **1985**, 4, 1819

[80] Widegren, J. A., Finke, R. G., *J. Mol. Catal. A: Chem.*, **2003**, 198, 317

[81] The activity of Rh(0) NPs were calculated from TOF values which is expressed as (mole of H_2 / (mole of rhodium x time)). Indeed, a rough calculation can be done to correct the catalytic activity of the second run. Since the size of Rh(0) NPs were found to be enlarged from 2.1 nm to 2.9 nm after the first cycle, only 72 % of initial Rh(0) NPs (2.1 nm) could be said to involve in the second cycle. Therefore, the corrected catalytic activity remained in the second cycle should be 83 % instead of 60 %.